High voltage, toughness and improved interfacial ion deposition through a dual-crosslinked and self-healable hydrogel electrolyte for green zinc-ion batteries

Yanping Yang [a,b,*], Luwei Shi [a], Yaqi Wu [a], Zhehua Chen [c], Xinyuan Zhu [b], Lijun Du [d,*], Youfu Wang [b,*]

[a] School of Materials Science and Engineering, Shanghai University of Engineering Science, Shanghai 201620, China
[b] School of Chemistry and Chemical Engineering, Shanghai Jiao Tong University, Shanghai 200240, China
[c] Shanghai Institute of Design and Innovation, Tongji University, Shanghai 200092, China
[d] Shanghai Huayi 3F New Materials Co., Ltd, Shanghai 200240, China

ARTICLE INFO

ABSTRACT

The inconsistent zinc stripping/deposition leading to low durability of zinc anodes is a fundamental obstacle for the practical application of zinc-based aqueous batteries. Hence, the self-healing capability of flexible batteries is crucial for enhancing their durability and dependability during routine operation, as it allows them to withstand various deformations. Through composite strengthening and dynamic coordination complexation, we have developed a dual-crosslinked and natural polymer-based self-healing hydrogel electrolyte (sodium carboxymethyl cellulose/sodium alginate-Zn^{2+}, denoted as CMC/SA-Zn^{2+}) for flexible Zn-MnO$_2$ batteries. The metal coordination interactions of carboxyl groups with Zn^{2+} as the dynamic motif are contributed to excellent mechanical and electrochemical properties, as well as fast self-healing ability for the CMC/SA-Zn^{2+} hydrogel electrolyte. Moreover, the improved compatibility of the electrode and electrolyte at their interfaces results in considerably more meticulous Zn deposition. Subsequently, a reversible plating/stripping performance is observed in a symmetric cell for a duration of 2000 h. After applying this self-healing and tough electrolyte to the flexible Zn-MnO$_2$ battery, it is constructed with a high capacity of 218 mAh/g and a high coulombic efficiency close to 100 %. Additionally, the flexible batteries exhibit exceptional resilience and can recover their electrochemical performance even after enduring multiple mechanical damages, highlighting their potential use in wearable electronics.

1. Introduction

Interest in quasi-solid-state power sources with superior electrochemical performance, safety, and environmental friendliness has surged due to the rising demand for secure electric vehicles, portable energy storage devices, and small electronic gadgets [1–7]. Among the various power sources investigated, flexible zinc-based aqueous batteries (FZABs) are considered to be one of the most promising alternatives because of their environmental friendliness and low cost of Zn element [8–15]. However, flexible energy storage devices encounter formidable challenges. Specifically, the conventional liquid electrolytes employ is susceptible to external pressures, leading to leakage and short circuits that compromise user safety [16,17]. In this regard, hydrogel offer a

viable solution by providing affordability, flexibility, self-healing properties, and stretchability. These properties enable effective control of Zn deposition/striping processes and regulation of interfacial ion transport, while also demonstrating resilience against collisions and sudden damage [18,19]. Consequently, the hydrogels emerge as highly promising candidates for gel electrolytes in flexible energy storage devices.

Significant advancements have been made in developing flexible zinc-based rechargeable batteries using hydrogel electrolytes in recent years. By incorporating materials like polyvinyl alcohol (PVA) [20], polyacrylamide (PAM) [21], hyaluronic acid (HA) [22], xanthan gum [23], and others, several promising flexible zinc-based batteries have shown excellent cycle stability. However, the mechanical properties and ion conductivity of conventional gel electrolytes based on a single-

---

network often fail to meet the required standards. In order to enhance both mechanical strength and ionic conductivity, one approach is to incorporate additives such as bacterial cellulose, nanocellulose, cotton cellulose, hydroxypropyl cellulose [24]. Another aspect pertains to the synergistic effects of multiple hydrogel networks, which comprise supramolecular chemical and physical cross-linked structures, thereby resulting in enhanced electrochemical performance of the flexible batteries. Chen et al. fabricated a borax crosslinked PVA/nanocellulose hydrogel electrolyte, and the assembled supercapacitors exhibited favorable mechanical properties and self-healing capabilities [25]. Li et al. synthesized a thermoreversible polymer hydrogel electrolyte (gelatin-g-PAM) that exhibits temperature-responsive sol–gel transition behavior, enabling high-performance zinc-ion batteries [26]. However, most reported double-network hydrogels are covalently cross-linked, lacking reversibility in case of cracks or breaks. Hydrogels must possess self-healing capabilities to enhance the longevity of manufactured electronics from a structural standpoint [27]. In addition, the voltage window of hydrogel electrolyte-based FZABs is typically limited to less than 2.0 V, and its preparation process is complex [28,29]. As a result, the development of high-voltage window and high energy density zinc-ion batteries is constrained compared to typical energy storage devices. Designing a type of self-healing polyelectrolyte with low cost and superior electrochemical performance is therefore crucial for FZABs.

Next-generation FZABs composed of natural polymer-based self-healing hydrogel electrolytes exhibit great potential for ecologically friendly materials because of their environmental friendliness, low cost, and degradability [30–34]. As a representative natural polymer and water-soluble polysaccharide, sodium carboxymethyl cellulose (CMC) is biocompatible, biodegradable and thermodynamically stable, rendering it a favored option for numerous applications as a gel polymer [35]. The carboxylate anion (–COO$^-$) groups in CMC are capable of facial cross-linking via ionic interactions with multivalent cations, resulting in gelation of CMC solutions [34,36]. The dynamic coordination between these two elements effectively enhances their performance and prolongs their lifespan, making them ideal for various applications where reliability is paramount [37,38]. For instance, Lin et al. conducted a study on the preparation of all-CMC sponges using an acid-assisted freeze-thawing technique. The results demonstrated the remarkable ability of these sponges to adsorb and subsequently re-adsorb heavy metal ions such as Ag$^+$, Cu^{2+}, and Ni^{2+} [39]. Furthermore, tough CMC hydrogel electrolytes can be prepared by sequentially crosslinking and acid-assisted freezing [40]. Unfortunately, the CMC-based hydrogel electrolyte used in those single-network requires acid-assisted freezing for preparation, leading to issues such as limited salt solubility, inadequate water absorption, low ionic conductivity, and weak self-healing ability. These limitations significantly impede the electrochemical performance of the battery. To address those challenges, we employ a direct, gentle,
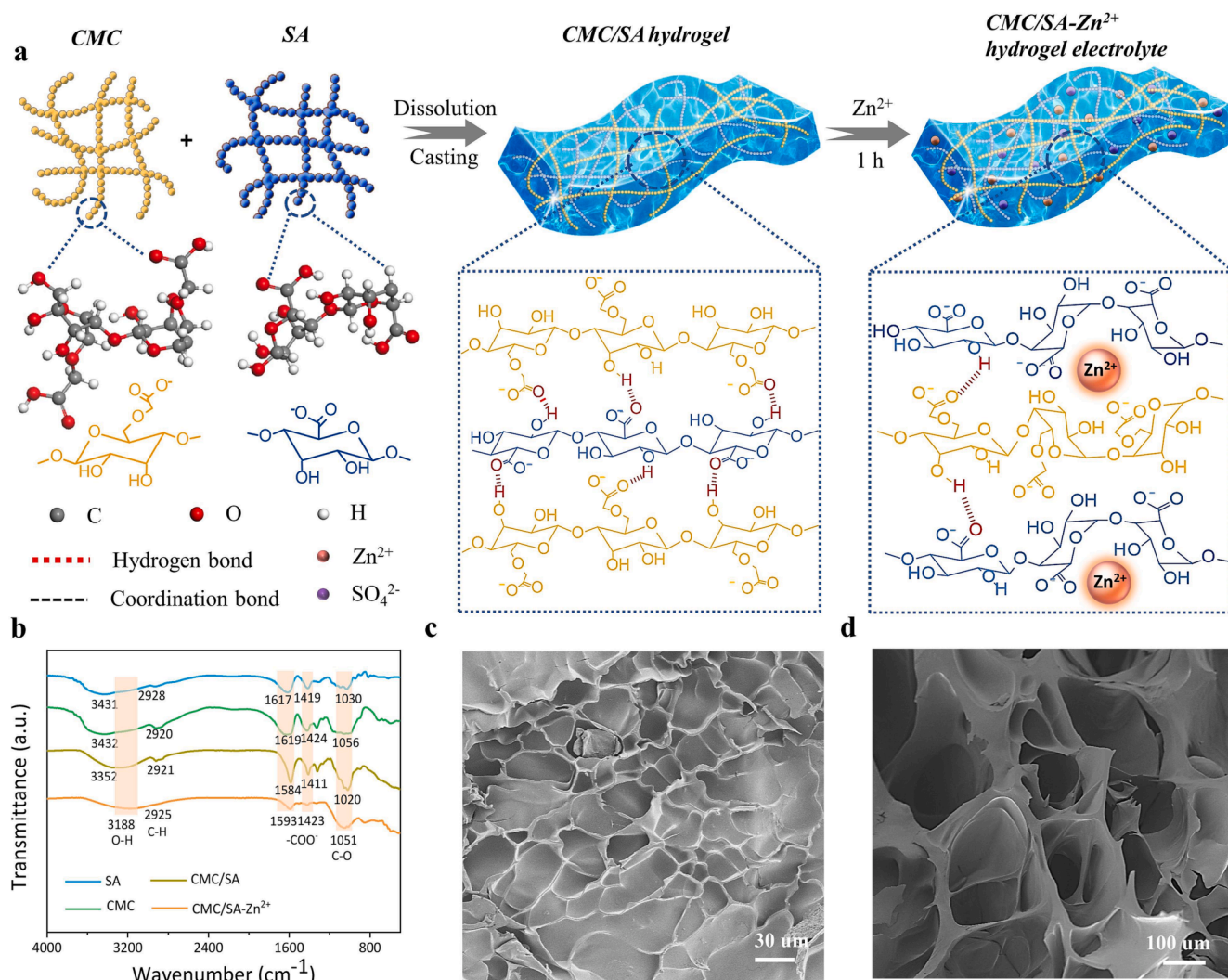
Fig. 1. (a) Synthesis schematic of the CMC/SA-Zn^{2+} hydrogel electrolyte. (b) FTIR spectra of SA, CMC, CMC/SA and CMC/SA-Zn^{2+}. (c) Surface, and (d) cross section SEM images of the CMC/SA-Zn^{2+} hydrogel electrolyte.

and rapid composite approach within our research framework to enhance the mechanical and/or other properties of CMC-based hydrogel systems. The chosen pathway excludes the use of petrochemical polymers and chemical crosslinking agents by incorporating sodium alginate (SA). This is because SA boast a polysaccharide structure similar to that of CMC, but with the added benefit of being incredibly hydrophilic [41]. Not only do they possess exceptional water absorption properties, but their hydroxyl groups also have the ability to form strong hydrogen bonds with CMC molecules. This unique interaction between SA and CMC results in a significant increase in the strength and durability of hydrogels as depicted in Fig. 1a. Furthermore, the dispersion of SA within this system adds an extra dimension to its toughening mechanism. Its abundant functional groups are also easy to crosslink with multivalent ions. The interplay between these two materials creates a synergistic effect that enhances their overall performance and effectiveness.

Herein, the CMC, SA, and ZnSO$_4$ salts were used to construct a double-network hydrogel electrolyte with high voltage, toughness and self-healing capability. Through a simple preparation process, CMC and SA chains were intertwined each other to form a hydrogel (CMC/SA) with a tangled network topology. The abundant functional groups present in the CMC/SA were subsequently ionic crosslinked with Zn^{2+} ions, leading to creation of a new high-performance hydrogel electrolyte (CMC/SA-Zn^{2+}). The replacement of Na$^+$ ions by Zn^{2+} ions played a crucial role in this process, as it allowed for molecular chain fragments to stack into an egg box structure at specific crosslinking points (Fig. 1a) [28]. These points served as anchors for the various chains within the hydrogel, providing additional strength and stability. Zn^{2+} could operate as both an ion-conducting agent and a cross-linking agent to facilitate the creation of the double cross-linked hydrogel electrolyte, which was necessary for the battery to function [42]. In comparison to the aqueous electrolyte, the CMC/SA-Zn^{2+} hydrogel electrolyte exhibited significantly improved Zn reversibility and enhanced durability, making it an ideal choice for flexible Zn-MnO$_2$ batteries. Not only does this hydrogel electrolyte deliveres high energy-storage performance, but it also has the ability to restore its energy-storage functions autonomously through dynamic reversible interactions, thereby demonstrating outstanding reliability and resilience. Our strategy enables the fabrication of all-natural polymer-based hydrogel electrolytes with multi-functionalities for mild FZABs possible, thereby expanding the utilization of natural biomaterials as highly safe, cost-effective and reliable alternative for flexible energy storage devices.

2. Experimental section

2.1. Materials and reagents

All chemical reagents, unless specifically stated differently, were purchased from commercial vendors and used without additional purification. Sodium carboxymethyl cellulose (CMC, MW: 700,000, DS = 0.9), sodium alginate (SA, AR), zinc sulfate heptahydrate (ZnSO$_4$·7H$_2$O) and manganese sulfate monohydrate (MnSO$_4$·H$_2$O, purity: 99.99 %) were purchased from Aladdin. Poly (vinylidene fluoride) (PVDF, MW: 900,000) and Super conducting carbon black (SP) were purchased from Taiyuan Lizhiyuan Battery Co., Ltd. Stainless steel mesh (500 mesh) was purchased from TianHong Co., Ltd.

2.2. Preparation of self-healable hydrogel electrolytes

To prepare CMC/SA-Zn^{2+} hydrogel electrolyte, 0.8 g CMC and 0.2 g SA were dissolved in deionized water, and then stirred well in a water bath at 60 °C to prepare a 2.5 % CMC/SA aqueous solution. The air bubbles were eliminated through centrifugation. Subsequently, the mixed solution was introduced into a polystyrene mold and subjected to partial water evaporation to yield the CMC/SA hydrogel. The resulting sample was then immersed in an aqueous solution containing 1.5 M

ZnSO$_4$ and 0.1 M MnSO$_4$ for 1 h to produce the CMC/SA-Zn^{2+} hydrogel electrolyte. For comparison, CMC-Zn^{2+} hydrogel electrolyte was prepared using a similar method as the CMC/SA-Zn^{2+} without the addition of SA. The liquid electrolyte (LE) was fabricated by mixing 1.5 M ZnSO$_4$ and 0.1 M MnSO$_4$ in 50 mL of deionized water, followed by stirring for 30 min for future application.

2.3. Preparation of the MnO$_2$ (manganese dioxide) cathodes

MnSO$_4$·H$_2$O (0.768 g) was dissolved in 15 mL of distilled water, followed by the gradual addition of 15 mL of 0.1 M KMnO$_4$ solution dropwise to the aforementioned MnSO$_4$ solution. After being stirred for 30 min, the mixture was carefully transferred to a hydrothermal reactor, specifically a Teflon-lined autoclave, where it was subjected to heat at 160 °C for 12 h. Following cooling to room temperature, the resulting product underwent further treatment by being centrifuged with deionized water three times before dried to yield MnO$_2$ nanorods [38].

MnO$_2$ cathodes were fabricated by blending MnO$_2$ nanorods, Super P, and polyvinylidene fluoride (PVDF) at a mass ratio of 7:2:1 in N-methyl pyrrolidone (NMP), followed by coating the mixture onto a metal mesh (Φ = 12 mm) for CR2032 coin cell and pouch battery, respectively. The active material-loaded substrates were then subjected to thermal treatment at 80 °C to obtain cathodes. Subsequently, the cathodes with 1 mg cm^{-2} α-MnO$_2$ nanorods were achieved.

2.4. Characterization

Field emission electron microscopy (FESEM, Sigma 300, Germany) with energy dispersive spectrometer (EDS, Oxford X-MAX20) was used to observe the surface morphologies and microstructure of electrodes and hydrogel electrolytes. The hydrogel electrolyte samples were subject to a 48 h process in a freezer dryer in order to eliminate water content, followed by sputtering with Au for SEM imaging prior to the experiment. The Thermo Fisher iCAP PRO was utilized for the conduction of ICP-OES (Inductively Coupled Plasma Optical Emission Spectrometer) spectroscopy. Images from optical microscope were captured using a PH50-1B43L-A/PL (Phenix, China) instrument. The chemical components were analyzed via Fourier transform infrared spectroscopy (FTIR, Nicolet 6700, America), while the mechanical properties were evaluated using a universal testing machine (LDW-5, China). The crystal structure was confirmed by X-ray diffraction (XRD) patterns with Cu Kα radiation (λ = 1.5406 Å).

2.5. Electrochemical analysis

Electrochemical impedance spectroscopy (EIS), linear sweep voltammetry (LSV), chronoamperometry (CA), and cyclic voltammetry (CV) were determined using an electrochemical workstation (CHI760E, CH Instruments Inc., Shanghai, China). Galvanostatic charge–discharge (GCD) measurements were performed on a battery testing system (CT-4008, Neware Electronics Co., Ltd, Shenzhen, China).

The ionic conductivity (σ) of the hydrogels was estimated using EIS measurements conducted by sandwiching the hydrogels between two stainless steel (SS) sheets. The test temperature was between 25 °C and 85 °C at an interval of 10 °C. The ionic conductivity is calculated by the following equation:

$$\sigma = \frac{d}{RA} \tag{1}$$

where σ (mS cm^{-1}) signifies the ionic conductivity of the hydrogel, A (cm^2) denotes the area of contact between the electrolyte and the electrodes, R (Ω) stands for the ohmic resistance obtained from impedance spectrum analysis, and d (cm) represents the distance between the two SS electrodes. Furthermore, the calculation of the activation energy Ea was based on the application of Arrhenius law (2):

$$\sigma = A\exp(-Ea/RT) \qquad (2)$$

where A represents the factor of frequency, Ea denotes the activation energy, R symbolizes the molar gas constant, and T signifies the absolute temperature.

The corrosion of Zn foil was assessed using a three-electrode setup, wherein the working electrode consisted of a Zn foil, the counter electrode was made of Pt foil, and a saturated Ag/AgCl electrode served as the reference electrode. The characterization involved performing LSV at a sweeping rate of 1 mV s^{-1}.

The electrochemical stability of CMC/SA-Zn^{2+}, CMC-Zn^{2+}, and liquid electrolyte (LE, *i.e.,* 1.5 M ZnSO$_4$ + 0.1 M MnSO$_4$ aqueous solution) was evaluated using the Zn//SS asymmetric cells *via* LSV. The voltage sweep was conducted at 0.1 mV s^{-1} from 0 to 3 V.

The zinc ion transference number ($t_{Zn^{2+}}$) of CMC/SA-Zn^{2+}, CMC-Zn^{2+}, and LE was determined through a combination of EIS and polarization measurements using the Zn//Zn symmetrical cells. A polarization bias ($\triangle V$) of 10 mV was applied to the cell to carry out the currents from the initial (I_0) to the steady state (I_s), the initial state impedance (R_0) and steady state impedance (R_s), respectively. The equation $t_{Zn^{2+}} = I_s (\triangle V\text{-}I_0R_0) / I_0(\triangle V - I_sR_s)$ was utilized for calculating the $t_{Zn^{2+}}$.

The CV curves of Zn/CMC/SA-Zn^{2+}/MnO$_2$ 2032-coin cell were obtained by scanning at a rate of 0.1 mV s^{-1} within the range of 0.8 V to 1.8 V.

The interfacial stability of the electrolyte/Zn metal was investigated by polarizing Zn/Zn symmetric cells with CMC/SA-Zn^{2+}, CMC-Zn^{2+} and LE, respectively. The cells were charged for 1 h and discharged for 1 h per cycle at constant current densities of 0.5 mA/cm^2, 2 mA/cm^2, and 5 mA/cm^2, respectively. Zn utilization rate was calculated by the following equation:

$$ZUR = \frac{C_{cycle}}{m \times C_{theoretical}} \times 100\% \qquad (3)$$

where C_{cycle}/mAh cm^{-2} is the specific capacity set for galvanostatic cycling, $C_{theoretical}$ is the theoretical gravimetric specific capacity (820 mAh/g) of Zn, and m (0.158 g) is the mass of the Zn working electrode. Therefore, Zn utilization rates at 0.5 mA/cm^2 (5.0 mAh/cm^2), 2 mA/cm^2 (2.0 mAh/cm^2), and 5 mA/cm^2 (5.0 mAh/cm^2), can be calculated as 4.4 %, 17.4 % and 43.6 %, respectively.

The Zn//Cu asymmetric cells were subject to charge–discharge at a current density of 1 mA/cm^2 with a capacity of 1 mAh/cm^2 and an upper voltage limit of 0.5 V, in order to evaluate the Coulombic efficiency of various electrolytes.

The specific capacity and cycling performance of Zn/CMC/SA-Zn^{2+}/MnO$_2$ batteries were evaluated by GCD measurements with a fixed charging time of 1 h and discharging time of 1 h, respectively. Specific capacity (mAh/g) of the FZMBs was calculation by the following equation (3):

$$C = \frac{I \times t \times 1000}{m} \qquad (4)$$

where I is the discharge current (A), t is the discharge time (h), and m is the mass of α-MnO$_2$ in the cathode (g).

2.6. Self-healing test

The CMC/SA-Zn^{2+} hydrogel electrolytes and flexible Zn-MnO$_2$ batteries (FZMBs) were bisected with a surgical blade and then meticulously reattached, allowing for autonomous self-repair over time. Additionally, the self-healing process and electrochemical performance of the healed CMC/SA-Zn^{2+} hydrogel electrolytes and FZMBs were evaluated.

2.7. DFT computational methods

The density functional theory (DFT) calculations were performed using the VASP code [43]. The Perdew–Burke–Ernzerhof (PBE) functional, based on the generalized gradient approximation (GGA) [44] was employed to handle the exchange–correlation effects. Additionally, a projector augmented-wave pseudopotential (PAW) [45] with a kinetic energy cut-off of 500 eV was utilized to accurately describe the expansion of the electronic eigenfunctions. The vacuum thickness was set to 25 Å in order to minimize interlayer interactions. A Γ-centered 5 × 5 × 5 Monkhorst–Pack k-point was used for Brillouin-zone integration sampling. All atomic positions were fully relaxed until energy and force reached a tolerance of 1 × 10^{-5} eV and 0.03 eV/Å, respectively. The dispersion corrected DFT-D method was employed to account for long-range interactions [46].

The binding energy (E_b) of a complex formed between two molecules A and B can be determined by employing the following equation:

$$E_b = E_{complex} - (E_A + E_B) \qquad (5)$$

where $E_{complex}$ is the total energy of the molecular complex of A and B. E_A and E_B are the total energies of isolated molecule A and B, respectively.

The Gibbs free energy change (ΔG) was calculated by computational hydrogen electrode (CHE) model as follows:

$$\Delta G = \Delta E + \Delta ZPE - T\Delta S \qquad (6)$$

where ΔE is the reaction energy obtained by the total energy difference between the reactant and product molecules absorbed on the catalyst surface, and ΔS is the change in entropy for each reaction, ΔZPE is the zero-point energy correction to the Gibbs free energy. T represents room temperature (298.15 K).

3. Results and discussion

3.1. Fabrication and investigation of the CMC/SA-Zn^{2+} hydrogel electrolyte

In general, the preparation of stable hydrogel electrolytes containing multivalent cations such as Zn^{2+} is challenging due to the tendency of polymer strands to aggregate in highly concentrated salt solutions [37,47]. Moreover, the kosmotropic characteristics of high concentrations of Zn^{2+} and specific anions, such as SO$_4^{2-}$, can weaken the hydrogen bonds within hydrogels. Consequently, this phenomenon led to changes in their physical properties and stability [48]. Fortunately, the development of the ionic cross-linked anionic polymer hydrogel electrolyte (CMC/SA-Zn^{2+}) can effectively address those challenges. The remarkable stability of the hydrogel network and its cross-linked structure can be attributed to the presence of a polyanionic chain, which is further reinforced by cross-linking with Zn^{2+}. Furthermore, the CMC/SA-Zn^{2+} hydrogel electrolytes possess abundant hydrophilic groups that effectively immobilize water molecules within the polymer skeleton, thereby minimizing side reactions. Additionally, the anionic polymers' charged groups have the ability to homogenize the ion distribution and facilitate uniform zinc deposition [49]. Consequently, the CMC/SA-Zn^{2+} hydrogel electrolytes demonstrate impressive mechanical properties, electrochemical performance, and intriguing self-healing capabilities.

As depicted in Fig. 1a, the CMC/SA-Zn^{2+} hydrogel electrolyte exhibits a dual-network architecture. The hydrophilic skeleton and functional groups of SA enable it to intertwine with CMC chains via hydrogen bonding, forming a web-like structure. Subsequently, ZnSO$_4$ is introduced to prepare an electrolyte that facilitates excellent ionic conductivity pathways, for which the hydrogel is able to efficiently transport ions and maintain its structural integrity. Free Zn^{2+} ions form ionic cross-links with the polar carboxyl or hydroxyl groups to create a

secondary physical cross-linking structure. In this egg box configuration, Zn^{2+} replace sodium ions and molecular chain fragments stack to establish crosslinking point. Zn^{2+} functions as a cross-linking agent and an electrolyte salt in the formation of a double cross-linked hydrogel electrolyte, thereby contributing to the preservation of mechanical and electrochemical properties in CMC/SA-Zn^{2+} through a facial and rapid immersion process for battery operation.

To uncover the interactions between molecules, such as hydrogen bonds and metal coordination within the hydrogel network, we recorded FTIR spectra of the CMC, SA, CMC/SA (without any salts), and CMC/SA-Zn^{2+}, as displayed in Fig. 1b. The peaks locate at 3432 cm^{-1} (O-H stretching vibration), 2920 cm^{-1} (C-H stretching vibration), 1619 cm^{-1} (stretching vibrations of symmetric –COO$^-$ groups.), 1424 cm^{-1} (stretching vibrations of asymmetric –COO$^-$ groups), and 1056 cm^{-1} (C-O stretching vibration in glucose units) are prominent characteristics of the functional groups of pristine CMC [50,51]. Similar bands with slightly varying placements can be seen in the case of SA. However, in the absence of any salts, a signature resembling that of CMC emerges due to the relatively low SA content present within the CMC/SA composite hydrogel. The –OH stretching peak exhibits a shift towards 3352 cm^{-1}, while the stretching vibration of symmetric and asymmetric –COO$^-$ groups shift to 1584 cm^{-1} and 1411 cm^{-1}, respectively. This indicates there are intermolecular interactions between macromolecular chains through hydrogen bonding [34]. The spectrum of the CMC/SA-Zn^{2+} hydrogel with $ZnSO_4$ + $MnSO_4$ electrolyte also shows similar shifts, as evidenced by the peaks shifting to 3188 cm^{-1}, 1593 cm^{-1}, and 1423 cm^{-1}, respectively. Furthermore, the peaks of hydroxyl and carboxyl functional groups in CMC/SA-Zn^{2+} are significantly attenuated compared to those in pristine CMC and CMC/SA composite hydrogel (without any salt), implying interactions between Zn^{2+} and functional groups of CMC and SA [27,52]. Besides, in comparison to the CMC-Zn^{2+}, the absorption peaks of –OH and –COO$^-$ functional groups in the CMC/SA-Zn^{2+} are more pronounced (Fig. S1, Supporting Information), indicating that stronger hydrogen and complex bonds have been formed within the CMC/SA-Zn^{2+} system. Consequently, it ultimately enhances the hydrophilicity of hydrogel electrolyte. Furthermore, the improved self-healing and mechanical property of the CMC/SA-Zn^{2+} hydrogel electrolyte can be attributed to the presence of reinforced dynamic hydrogen and metal coordination bonds. Moreover, the high hydrophilicity plays a crucial role in enhancing interfacial compatibility of the CMC/SA-Zn^{2+} hydrogel electrolyte. After undergoing erosion caused by expansion of ice crystals during vacuum freeze-drying, the CMC/SA-Zn^{2+} displays a significantly more porous 3D structure compared to that of CMC-Zn^{2+} hydrogel electrolyte as shown in Fig. 1(c, d) and Fig. S2 (Supporting Information). The corresponding EDS elemental mapping analysis in Fig. S3 (Supporting Information) demonstrates the uniform distribution of elements C, O, and Zn within the CMC/SA-Zn^{2+} hydrogel electrolyte. Moreover, the ICP-OES analysis reveals that the Zn^{2+} content in the CMC/SA-Zn^{2+} hydrogel electrolyte is approximately 21.3 wt %. In addition, CMC/SA-Zn^{2+} hydrogel electrolyte develops a highly porous structure with an average pore size of approximately 100 um (Fig. 1d). These pores serve as ion migration channels that enhance Zn^{2+} ions transport, and thus contributing to exceptional ionic conductivity.

3.2. Mechanical properties and self-healing behavior of the CMC/SA-Zn^{2+} hydrogel electrolyte

The typical strain–stress curves, as shown in Fig. 2a, were used to assess the mechanical properties of the CMC/SA-Zn^{2+} and CMC-Zn^{2+} hydrogel electrolyte as it was initially prepared. The as-prepared CMC/SA-Zn^{2+} hydrogel electrolyte exhibits a high tensile strength of 1.42 MPa under 134 % strain and toughness of 512.8 kJ m^{-3}, while the corresponding values of CMC-Zn^{2+} is only 0.80 MPa under 127 % strain and 455.0 kJ m^{-3}, respectively (Fig. 2a, b). Furthermore, the CMC/SA-Zn^{2+} hydrogel electrolyte demonstrates excellent resilience and high stretchability of up to approximately 100 % strain even after undergoing

20 twisting tests (Fig. 2c), which owing to the presence of hydrogen bonds and coordination bonds within the 3D network. In other words, this unique cross-linked network facilitates easy reconnection after external force is applied, while preserving the structural integrity of the CMC/SA-Zn^{2+} hydrogel electrolyte. Interestingly, the mechanical strength of CMC/SA-Zn^{2+} also surpass that of many reported gel-electrolyte-based devices as described in Fig. 2d and Table S1 (Supporting information). It is well known that hydrogel electrolytes are often prioritized for their high stretchability in these literature studies. However, the low fracture strength of these materials may increase the risk of short circuits when the batteries are bent [53]. In contrast, the CMC/SA-Zn^{2+} hydrogel electrolyte exhibits significantly higher fracture stress of up to 1.42 MPa while maintaining comparable stretchability (134 %). The significant enhancement in mechanical robustness of the CMC/SA-Zn^{2+} hydrogel electrolyte can be primarily attributed to the strengthened electrostatic attraction between chains and the restructuring of hydrogen and metal coordination bonding network induced by SA. These factors encourage the development of a composite hydrogel electrolyte for superior strength and adaptability.

Moreover, no visible yield point is observed during the tensile tests, setting it apart from other highly stretchable materials [18]. The exceptional characteristic of this phenomenon may be ascribed to the comparatively low molecular weights (MWs) of both CMC and SA polymers, combined with the coordination nature of the CMC/SA-Zn^{2+} complexes, which exhibits a striking similarity to Bao's work in this field [54]. The addition of Zn^{2+} ions into a hydrogel structure results in the formation of coordination bonds that act as dynamic cross-linkers between inter-chains. These bonds are highly responsive and can quickly break and reform when the hydrogel is stretched, allowing for greater flexibility and adaptability. Further measurements of the adhesion of Zn foil to CMC/SA-Zn^{2+} hydrogel electrolyte was conducted as shown in Fig. S4 in the Supporting Information. The Zn foil was attached to one end of a hydrogel electrolyte composed of CMC/SA-Zn^{2+}, while the remaining ends of these two components were securely fastened together. We tried to separate the Zn foil from the CMC/SA-Zn^{2+} hydrogel electrolyte by adjusting the upper clamp. Surprisingly, it couldn't detach the Zn foil from the CMC/SA-Zn^{2+} hydrogel electrolyte. Instead, when we stretched the CMC/SA-Zn^{2+}, it eventually broke, indicating a strong adhesion between these components that exceeds the tensile strength of CMC/SA-Zn^{2+} hydrogel electrolyte. This remarkable adhesion property ensures a close contact with Zn electrodes, enabling devices to withstand significant deformations and enhancing the overall performance and reliability [34].

The microscopic features were identified to further elucidate the self-healing property. Fig. 2e shows a schematic diagram of self-healing process within CMC/SA-Zn^{2+} hydrogel electrolyte. The material is cut into two parts, and then triggers the natural healing process by the dynamic ionic interaction between –COO$^-$ and Zn^{2+}, as well as hydrogen-bonding interaction. Meanwhile, we divided the as-prepared gel electrolytes with and without rhodamine B (Fig. 2f (I)) into two parts with a scalpel to further confirm the self-healing phenomena. The presence of rhodamine B allows for a clear demarcation at the fresh cut interface (Fig. 2f (II)), as opposed to a diffuse and indistinct boundary. Upon contact, two pieces of CMC/SA-Zn^{2+} hydrogel electrolyte (*i.e.,* the normal and dyed gel electrolyte) rapidly fuse together, and dye diffusion occurs from the dye-doped to the dye-undoped block (Fig. 2f (III)), demonstrating the self-healing and self-sustaining nature of the electrolyte. To illustrate more clearly the self-healing behavior of the CMC/SA-Zn^{2+} hydrogel electrolytes, the morphological changes of scratches on the surface of the CMC/SA-Zn^{2+} hydrogel electrolyte were studied using optical microscopy (Fig. 2g). The scratches gradually disappear over time, demonstrating the autonomously self-healing ability of the CMC/SA-Zn^{2+} hydrogel electrolyte in ambient air without any external stimuli or healing agents [55]. In contrast, after 72 h, the CMC/SA hydrogel without Zn^{2+} exhibited incomplete repair, with clearly visible unrepaired scratches at the interface, indicating a weak repair capability
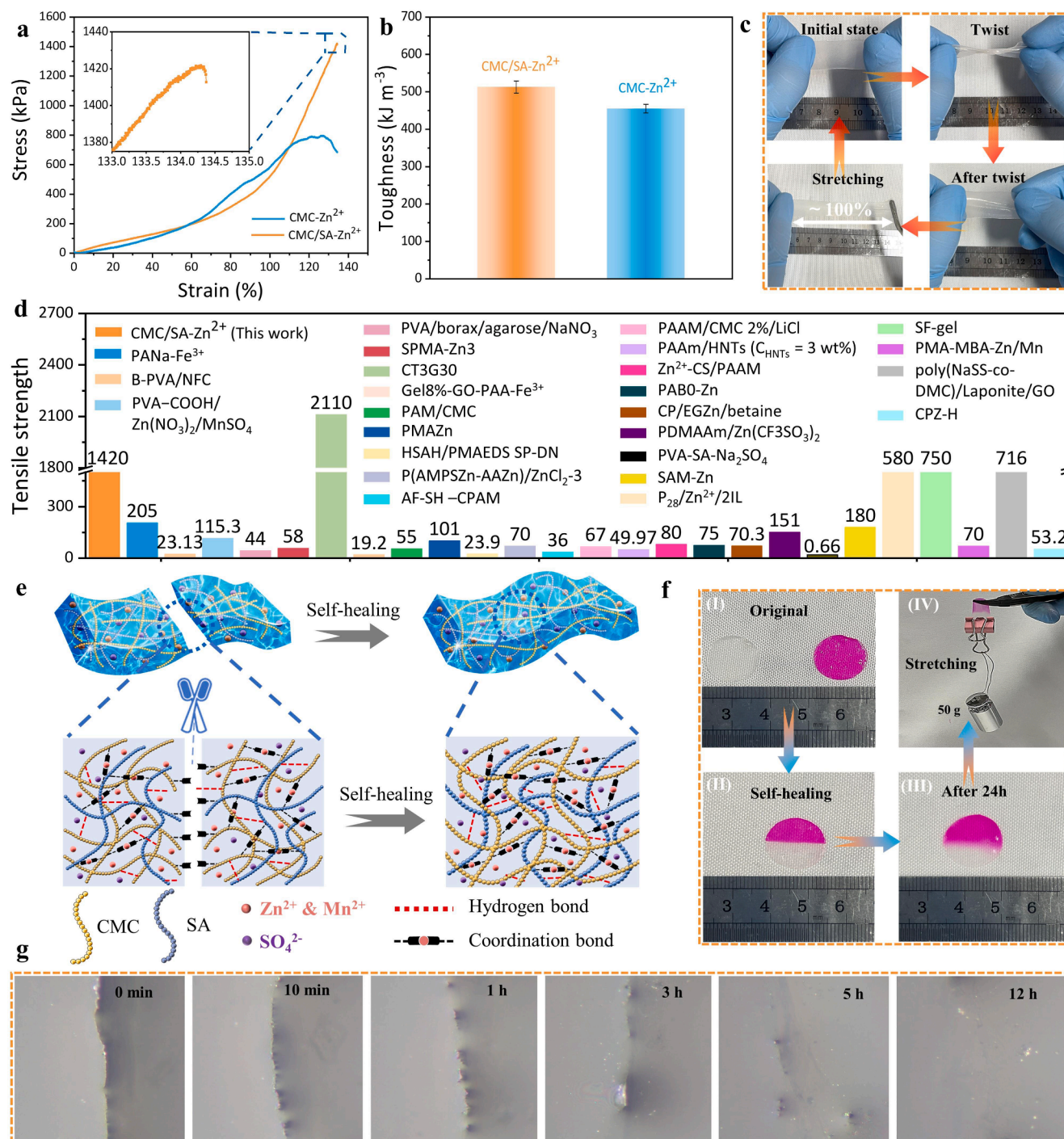
Fig. 2. (a) Tensile σ-ε curves and (b) toughness comparison of the CMC/SA-Zn^{2+} and CMC-Zn^{2+} hydrogel electrolytes. (c) Optical photographs of twisting and stretching test of the CMC/SA-Zn^{2+} hydrogel electrolyte. (d) Comparison of tensile strength with previously reported hydrogel electrolytes. (e) Composition and self-healing illustration, optical images of (f) self-healing behavior and (g) process of the CMC/SA-Zn^{2+} hydrogel electrolyte.

attributed to single hydrogen bond interactions (Fig. S5, Supporting Information). It suggests that self-healing properties of CMC/SA-Zn^{2+} hydrogel is significantly enhanced by the introduction of Zn^{2+}, which facilitates dynamic ionic coordination formation. The double-network structure, established through the synergistic effect of dynamic ionic coordination and hydrogen bonding, enhances the self-healing properties of CMC/SA-Zn^{2+} hydrogel electrolyte.

To verify the electrochemical properties of the self-healing gel electrolyte, it is necessary to conduct an investigation into its ionic conductivity of the CMC/SA-Zn^{2+} hydrogel electrolyte. We utilize the

highly effective alternating current (AC) impedance method and test the CMC/SA-Zn^{2+} at different numbers of cutting/self-healing cycles. As depicted in Fig. S6 (Supporting Information), the ionic conductivity of the resulting self-healing gel electrolyte experiences a slight decrease, yet remains within the same order of magnitude as that of its initial state even after undergoing four cutting/self-healing cycles. Furthermore, a tensile test using forceps demonstrates that the gel electrolyte is capable of supporting a mass of 50 g after healing (Fig. 2e (IV)), indicating the reformation of its network and restoration to its original mechanical strength level. These characteristics are crucial for utilizing the CMC/

SA-Zn^{2+} hydrogel as self-repairing electrolytes for FZABs, which require stable and efficient ion transport to function effectively.

3.3. Electrochemical properties and Zn deposition behavior of the Zn/CMC/SA-Zn^{2+} anode

A crucial prerequisite for the advancement of zinc-ion battery technology is the enhancement of electrochemical performance and stability at the electrolyte–electrode interface. However, the formation of zinc dendrites and parasitic side reactions pose significantly obstacles to the development of FZABs.[49] Hence, it is unsurprising that Zn/Zn symmetric cells utilizing a conventional liquid electrolyte (LE, *i.e.,* an aqueous solution of 1.5 M ZnSO$_4$ + 0.1 M MnSO$_4$) exhibit unstable performance, as illustrated in Fig. 3a. At a current density of 0.5 mA/cm^2, the deposition potential of the Zn/LE/Zn symmetric cell is approximately 42 mV at the initial stage. Nevertheless, large overpotential along with large irreversible voltage drop at 400 h (*i.e.,* 200 cycles) is observed in the symmetric cell. The abrupt failure may
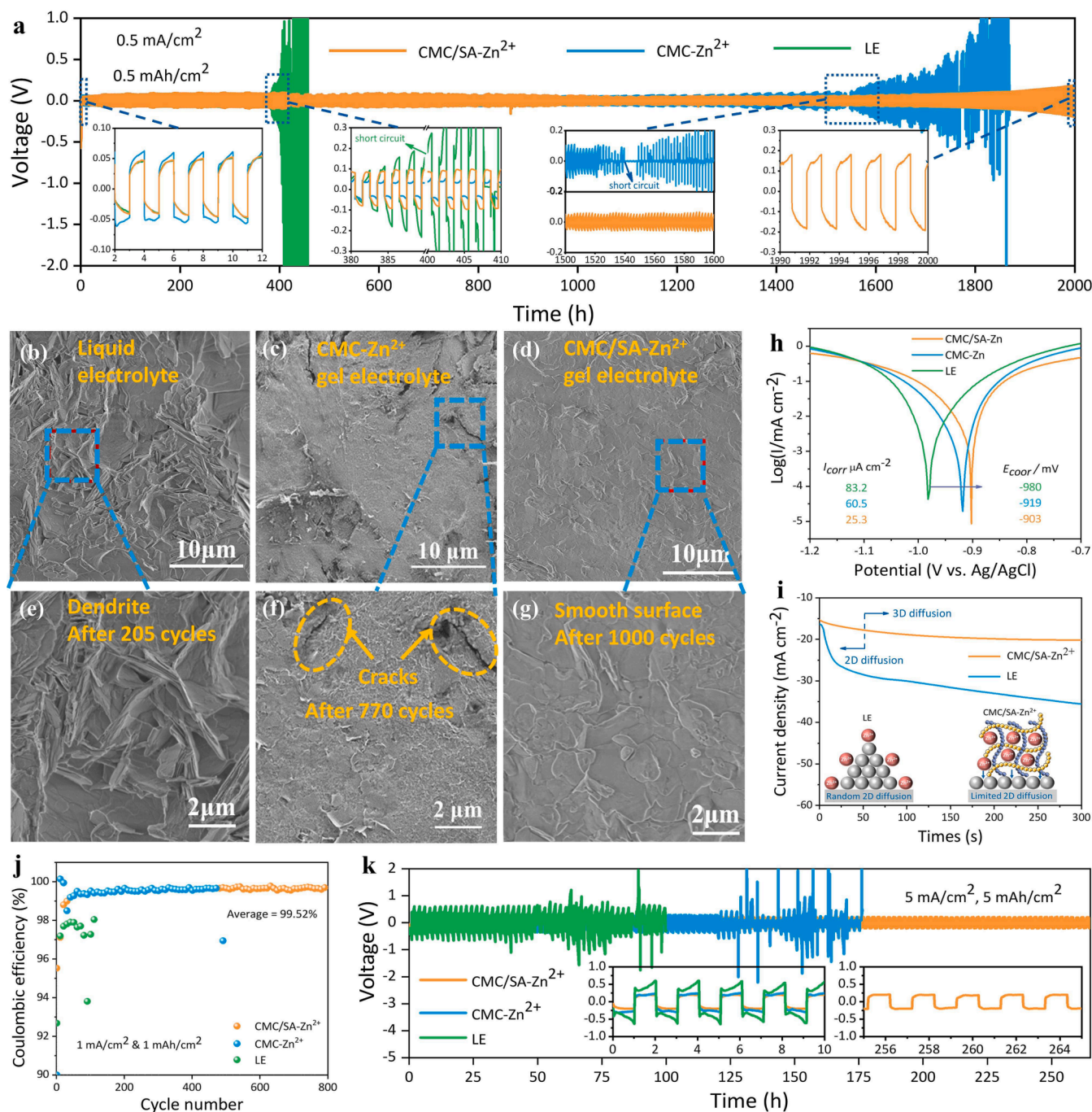
Fig. 3. (a) Symmetric cycling performance of Zn/CMC/SA-Zn^{2+}/Zn, Zn/CMC-Zn^{2+}/Zn and Zn/LE/Zn cells under the current density of 0.5 mA/cm^2. SEM images of the Zn metal anodes after plating/stripping in the liquid electrolyte (LE) (b, e), CMC-Zn^{2+} hydrogel electrolyte (c, f) and CMC/SA-Zn^{2+} hydrogel electrolyte (d, g). (h) Tafel curves in LE, CMC-Zn^{2+} and CMC/SA-Zn^{2+} electrolyte. (i) Chronoamperograms of Zn/CMC/SA-Zn^{2+}/Zn and Zn/LE/Zn cells at a −150 mV overpotential. Insets: types of Zn^{2+} diffusion and reduction process. (j) Long-term cyclic performance of Zn//Cu asymmetric cells in LE, CMC-Zn^{2+} and CMC/SA-Zn^{2+} electrolyte under 1 mA/cm^2 with a capacity of 1 mAh/cm^2. (k) Symmetric cycling performance of Zn/CMC/SA-Zn^{2+}/Zn, Zn/CMC-Zn^{2+}/Zn and Zn/LE/Zn cells under the current density of 5 mA/cm^2.

probably due to uncontrolled dendrite growth and overgrowth of inert ZSHs (zinc sulfate hydrates) byproduct that passivates the Zn electrodes, implying the occurrence of short circuit [20,34]. In contrast, the symmetrical Zn/CMC/SA-Zn²⁺/Zn cell remains the initial deposition potential of 42 mV, and ultra-long deposition potential of 90 mV for more than 1800 h (*i.e.*, 900 cycles) at the steady stage (Fig. S7, Supporting Information). Furthermore, the time–voltage curve retains its shape even after 2000 h (1000 cycles) as shown in Fig. 3a. This is also significantly better than that of the symmetric Zn/CMC-Zn²⁺/Zn cell (only undergoing 1540 h of cycling). Therefore, the effectiveness of the CMC/SA-Zn²⁺ hydrogel electrolyte in inhibiting of zinc dendrites and inert byproducts is highly manifested.

The zinc surface was further observed using SEM, revealing a distinct protruding surface morphology with abundant deposited zinc dendrites in the presence of liquid electrolyte (205 cycles, Fig. 3b, e) and the occurrence of obvious cracks in the CMC-Zn²⁺ hydrogel electrolyte (770 cycles, Fig. 3c, f). Furthermore, even after 1000 cycles in CMC/SA-Zn²⁺, a dense deposition morphology with a smoother and dendrite-free Zn anode is still observed (Fig. 3d, g). The enhanced deposition of Zn onto the Zn (002) crystal plane during the plating/stripping process can be ascribed to the stronger adsorption energy of the CMC/SA complex along this specific plane (Fig. 4a). This suggests that the synergistic effect of the CMC and SA in the CMC/SA-Zn²⁺ hydrogel electrolyte plays a crucial role in promoting efficient Zn deposition [2].

Additionally, in Fig. 3h, the Tafel corrosion potentials (E_{coor}) *vs.* Ag/AgCl of Zn plates in LE, CMC-Zn²⁺, and CMC/SA-Zn²⁺ are −980, −919 and −903 mV with corrosion current densities (I_{coor}) of 83.2, 60.5, and 25.3 uA cm⁻², respectively. The observed decrease in corrosion current density implies a slower reaction kinetics of Zn plating/corrosion when

immersed in hydrogel electrolytes. This finding highlights the unique anti-corrosive characteristics of the as-prepared CMC/SA-Zn²⁺ hydrogel electrolyte. The slower reaction rate indicates that the hydrogel electrolyte provides a protective barrier against corrosion, preventing or minimizing damage to the zinc metal.

The growth mechanism of the Zn deposit at the interfacial sites between the hydrogel electrolyte/Zn was further examined by chronoamperometry (CA). The current response, which is influenced by the formation of nucleation centers, was recorded over time for Zn ‖ Zn cells with both LE and CMC/SA-Zn²⁺ hydrogel electrolyte at an overpotential of −150 mV, as depicted in Fig. 3i. The CMC/SA-Zn²⁺ hydrogel electrolyte achieves a steady current density after 51 s, whereas the cell with LE continues to increase beyond 250 s. This indicates that the extensive and rampant 2D diffusion process observed in LE can be mitigated when utilizing the CMC/SA-Zn²⁺ hydrogel electrolyte. The absorption of Zn²⁺ is well known to result in their horizontal spreading across the surface and accumulate at sites that offer the optimal conditions for charge transfer, such as defective area or tip sites [2,56,57]. Consequently, they have a tendency to form rampant dendrites in order to minimize the energy of the surface and reduce its expose area on the interface of Zn-LE. This behavior can be attributed to the sluggish diffusion of Zn and its limited compatibility in the liquid electrolyte interface. As a contrast, the abundant Zn²⁺ transport channels present in the CMC/SA-Zn²⁺ hydrogel electrolyte with a robust interface can ensure uniform Zn²⁺ flux, thereby achieving the stable accumulation of Zn²⁺ on Zn metal in a 3D spatial manner (the inset in Fig. 3i). We conducted further experiments on the Coulombic efficiency of Zn‖Cu cells and the higher current densities (2 mA/cm² and 5 mA/cm²) of Zn‖Zn symmetric cells, as shown in Fig. 3j, Fig. S8 (Supporting Information) and Fig. 3k. The
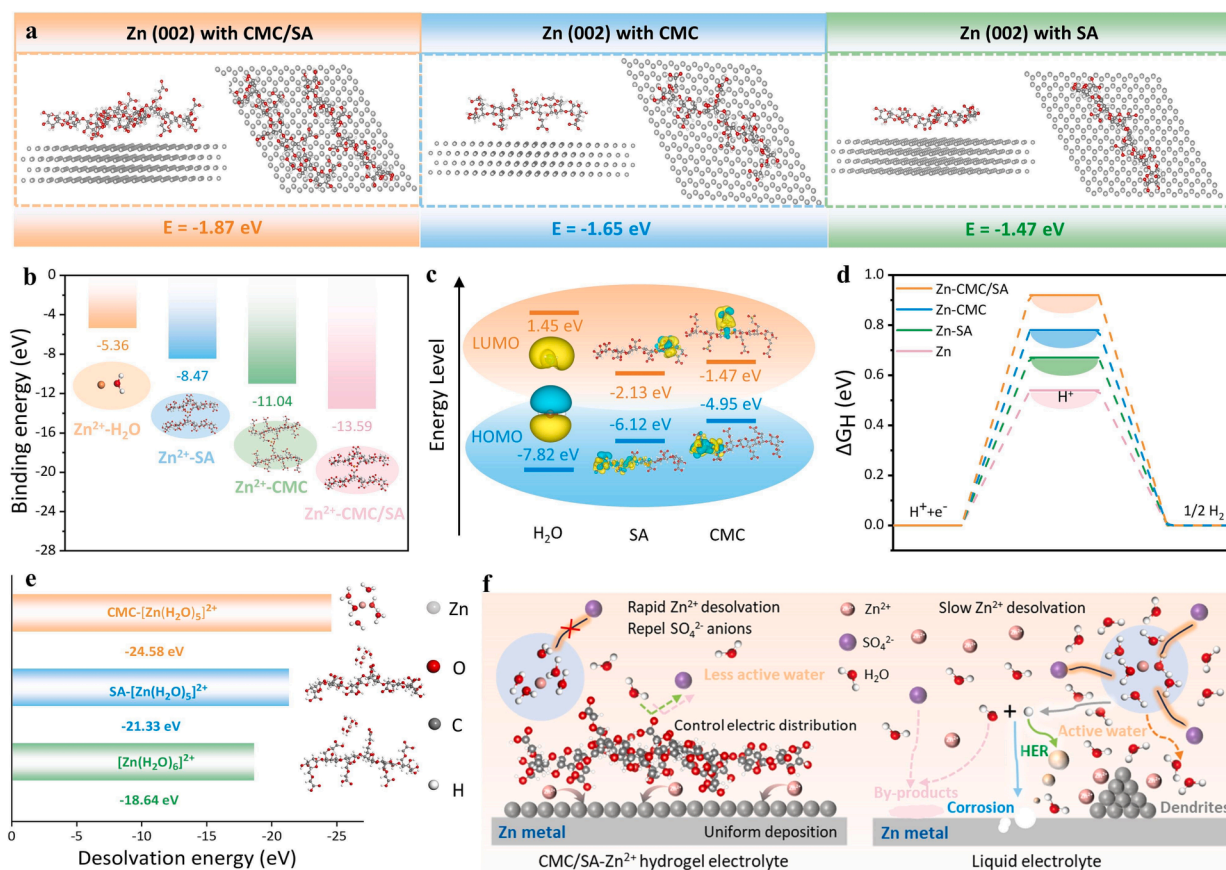
Fig. 4. (a) Adsorption energy of the SA, CMC and CMC/SA to Zn (002) plane. (b) Binding energies of Zn²⁺–H₂O, Zn²⁺-SA, Zn²⁺-CMC, and Zn²⁺-CMC/SA. (c) Molecular orbital energies of H₂O, SA and CMC molecules. (d) ΔG_H of Zn-CMC/SA, Zn-CMC, Zn-SA and bare Zn. (e) Desolvation energies of CMC-[Zn(H₂O)₅]²⁺, SA-[Zn(H₂O)₅]²⁺ and [Zn(H₂O)₆]²⁺. (f) Schematic illustration of the regulation mechanism of CMC/SA-Zn²⁺ hydrogel electrolyte and liquid electrolyte on Zn electroplating.

findings demonstrate that the hydrogen evolution reaction (HER) and associated corrosion reactions are effectively suppressed by the CMC/SA-Zn^{2+} hydrogel electrolyte, attributed to the diminished water activity and enhanced electrochemical stability. The Zn//Cu cell exhibits a remarkable enhancement in the efficiency of Zn plating/stripping when using the CMC/SA-Zn^{2+} hydrogel electrolyte. It achieves an average Coulombic efficiency of 99.5 % after undergoing 800 cycles at 1 mA/cm^2 with the capacity of 1 mAh/cm^2 (Fig. 3j). The cycle performance of the Zn anode under a current density of 2 mA/cm^2 (*ZUR* of 17.4 %) and 5 mA/cm^2 (*ZUR* of 43.6 %) was further investigated in order to assess the potential of the CMC/SA-Zn^{2+} hydrogel electrolyte for practical applications. The Zn//Zn symmetric cell employing CMC/SA-Zn^{2+} hydrogel electrolyte demonstrates consistent cycling performance for 700 h at a current density of 2 mA/cm^2 (Fig. S8, Supporting Information) and maintains stability for up to 250 h even at a higher current density of 5 mA/cm^2 (Fig. 3k). This remarkable performance achieved by our CMC/SA-Zn^{2+} hydrogel electrolyte is surprisingly comparable to that of state-of-the-art cells utilizing gel electrolytes (Table S2, Supporting Information), demonstrating its potential for practical applications in wearable or implanted devices.

The theoretical binding energies of the carboxyl anionic groups of CMC and SA in the CMC/SA-Zn^{2+} hydrogel electrolyte (-13.59 eV) for Zn^{2+} are surpass that of H_2O (-5.36 eV) for Zn^{2+}, indicating the superior affinity of CMC and SA towards Zn in the CMC/SA-Zn^{2+} hydrogel electrolyte (Fig. 4b). This finding indicates that selective capture of Zn^{2+} and repulsion of SO_4^{2-} by anionic functional groups may be highly advantageous. The effects of the lowest unoccupied molecular orbital (LUMO) and highest occupied molecular orbital (HOMO) levels on the thermodynamic stability of batteries were further characterized. The LUMO energy of H_2O molecules (1.45 eV), as depicted in Fig. 4c, exhibits a significantly more positive value compared to that of SA (-2.13 eV) and CMC molecules (-1.47 eV) in the CMC/SA-Zn^{2+} hydrogel electrolyte. This observation suggests that the reduced LUMO level of the CMC/SA-Zn^{2+} hydrogel electrolyte effectively inhibits the spontaneous reduction of H_2O molecules, specifically referring to the HER process. Moreover, the higher value of ΔG_H for Zn-CMC/SA reveals that water dissociation on the Zn/CMC/SA-Zn^{2+} anode is more challenging in comparison to the bare Zn anode due to the presence of CMC and SA. Consequently, the CMC/SA-Zn^{2+} hydrogel electrolyte can further restrict proton availability, and then hinder H_2 generation and evolution (Fig. 4d). In addition, it is well recognized that the Zn^{2+} solvated shells in an electrolyte hinder the movement of ions and impede charge transfer between electrodes during electrochemical reactions. Therefore, the desolvation of Zn^{2+} plays a crucial role in facilitating charge transfer in electrochemical systems. As shown in Fig. 4e, the desolvation energies of CMC-$[Zn(H_2O)_5]^{2+}$ and SA-$[Zn(H_2O)_5]^{2+}$ (representing the simplified solvation environment in the CMC/SA-Zn^{2+} hydrogel electrolyte) are -24.58 and -21.33 eV, respectively, which is finding to be more negative than that of $[Zn(H_2O)_6]^{2+}$ (-18.64 eV). This emphasizes that the CMC/SA-Zn^{2+} hydrogel electrolyte has a stronger ability to remove solvent molecules from zinc ions, consistent with its higher transfer number of zinc ion ($t_{Zn^{2+}}$), which will be discussed later [2].

Based on the above discussion, the uniform deposition at the interface of Zn-CMC/SA-Zn^{2+} may be due to the fact that CMC/SA-Zn^{2+} effectively reduces corrosion and side reactions by immobilizing water molecules through electrostatic and hydrogen bonding interactions. Furthermore, the abundant Zn^{2+} transport channels and the unique zincophilic properties of anionic polymers' charged groups can homogenize the ion distribution and limit the 2D diffusion to facilitate uniform deposition of zinc. The synergistic effect results in excellent long cycle performance of the Zn/CMC/SA-Zn^{2+}/Zn symmetric cell (Fig. 4f).

According to the AC impedance spectroscopy and Equation (1), the resistance and corresponding ionic conductivity of the CMC/SA-Zn^{2+} hydrogel electrolyte at different temperatures have been shown in Fig. S9a and Fig. S10 (Supporting Information). As the resistance of the as-prepared electrolyte decreases, the ionic conductivity gradually improves (2.08 mS cm^{-1} to 5.73 mS cm^{-1}) with the increase of temperature (25 °C to 85 °C), and vice versa. This phenomenon may be attributed to the increase in the kinetic energy of the carriers as the temperature increasing, which is very common in ionic conducting conductors [27]. Furthermore, based on the Arrhenius equation ($\sigma = A\exp(-Ea/RT)$), the CMC/SA-Zn^{2+} shows an activation energy (*Ea*) of 16.96 kJ mol^{-1}, which is smaller than that for the CMC-Zn^{2+} hydrogel electrolyte (21.04 kJ mol^{-1}) and higher than that for LE (7.08 kJ mol^{-1}) (Fig. 5a and Fig. S9, Supporting Information). The relatively lower *Ea* of the CMC/SA-Zn^{2+} hydrogel electrolyte suggests a reduced barrier to ion transport, thereby facilitating accelerated ion transportation and minimizing electrode polarization, and then enhancing the electrochemical performance of Zn electrodes. To investigate the electrochemical stability window of the electrolytes, Zn/CMC/SA-Zn^{2+}/stainless steel, Zn/CMC-Zn^{2+}/stainless steel, and Zn/LE/stainless steel cells were prepared and characterized by linear scanning voltammetry (LSV) at 25 °C. The anodic current observed in the current–voltage curve corresponds to the electrochemical oxidative decomposition as described in Fig. 5b. The CMC/SA-Zn^{2+} shows a broader electrochemical stability window than that of CMC-Zn^{2+} and LE, especially in the positive direction. Furthermore, no observable oxidation current is detected for Zn/Zn^{2+} up to 2.4 V, indicating the potential application of the CMC/SA-Zn^{2+} hydrogel electrolyte in high-voltage zinc-ion battery packs with a stable and wide potential window. Moreover, compared to most hydrogel electrolytes (Table S3, Supporting Information), CMC/SA-Zn^{2+} exhibits a superior electrochemical window. The abundance of hydrophilic and charged groups, as well as hydrogen bond interactions, may be the main cause for the widening of the electrochemical window. These factors increase the binding force of free H_2O molecule and effectively hider their movement and decomposition. Therefore, both hydrogen evolution and oxygen evolution voltages are elevated, leading to decreased reaction activity in the as-prepared hydrogel electrolyte [28]. The transfer number of zinc ion ($t_{Zn^{2+}}$) is also a crucial factor on the performance of hydrogel electrolyte, as low $t_{Zn^{2+}}$ leads to increased electrode polarization and reduced cell performance. The Vincent and Evans method was employed to calculate $t_{Zn^{2+}}$ for CMC/SA-Zn^{2+}, CMC-Zn^{2+}, and LE as shown in Fig. 5c. The corresponding polarization curves and EIS images of pre-polarization and post-polarization were shown in Fig. S11-S13 (Supporting Information). The cell was subjected to a polarization bias ($\triangle V$) of 10 mV, and the resulting change in current over time was recorded. After 2000 s, the current during the polarization process reached a plateau, indicating that a steady-state current had been achieved. The value of $t_{Zn^{2+}}$ for CMC/SA-Zn^{2+} is 0.72, which represents a significantly increase compared to that observed in the CMC-Zn^{2+} hydrogel electrolyte (0.54) and LE (0.22), implying that the introduction of SA into the CMC/SA-Zn^{2+} greatly enhances Zn^{2+} conduction behavior [49].

3.4. Electrochemical performance of the Zn-MnO$_2$ batteries with CMC/SA-Zn^{2+} hydrogel electrolyte at room temperature

The selection of cathode materials plays a crucial role in determining the cost and electrochemical performance of AZIBs [58,59]. Currently, the researches focus on finding cathode materials that can effectively undergo Zn intercalation/de-intercalation with high reversibility, specifically using Mn-based cathodes [22,34], V-based cathodes [15,57], Prussian blue analogues-based cathodes [60,61], organic-based cathodes [42,62], layered transition metal dichalcogenides-based cathodes [63,64], other metal oxides-based cathodes [65,66], polyanionic compounds-based cathodes [67,68], and halogen-based cathodes [69,70]. Among these, MnO_2 serves as a promising water-based cathode material and can be well paired with zinc metal anodes [71,72].

Therefore, the electrochemical performance of the CMC/SA-Zn^{2+} hydrogel electrolyte was further evaluated in flexible Zn-MnO$_2$ batteries
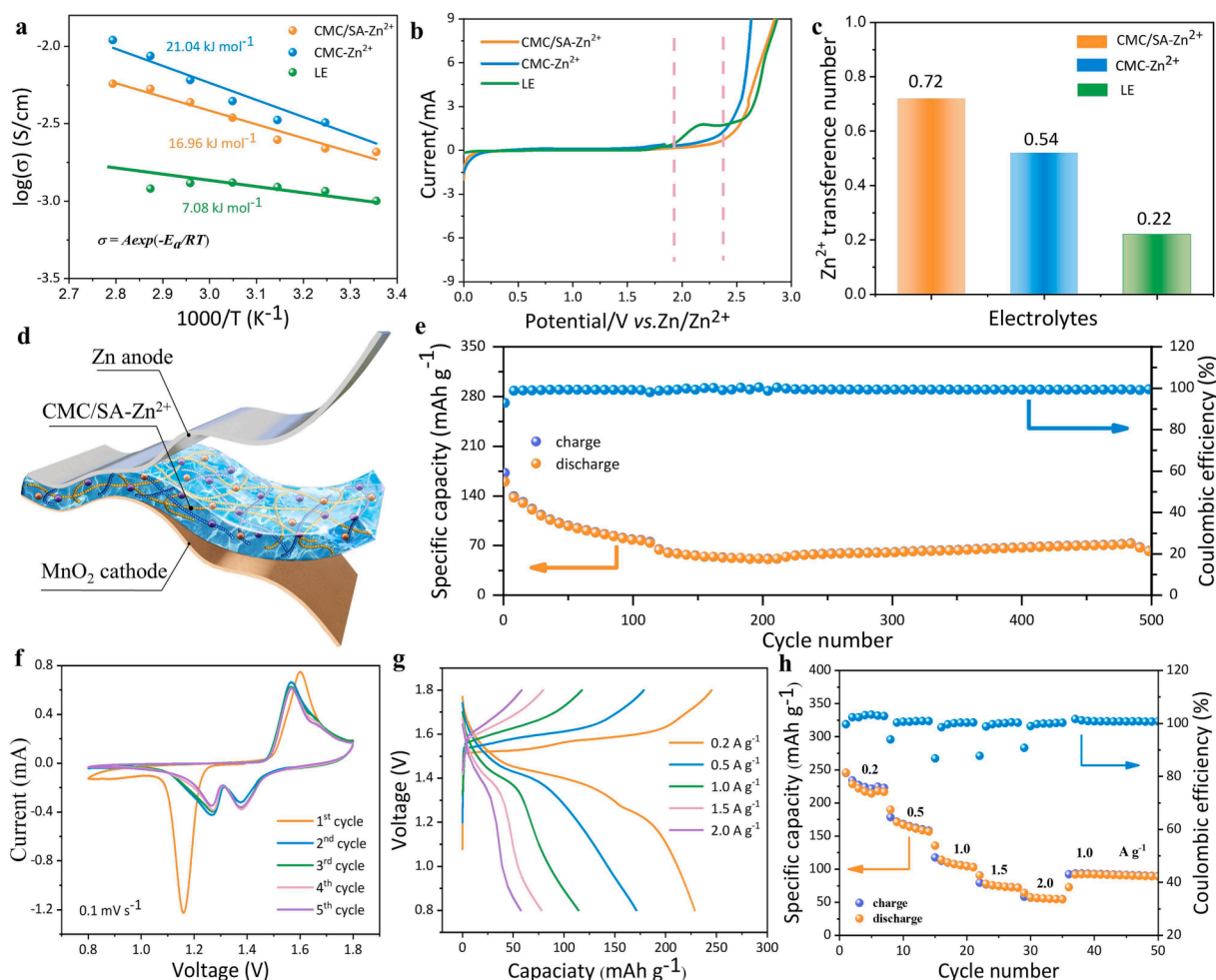
Fig. 5. (a) Corresponding Arrhenius plots and comparison of activation energies, (b) LSV curves with a scan rate of 0.1 mV s^{-1} from 0 to 3 V, and (c) transference number of Zn^{2+} in the CMC/SA-Zn^{2+}, CMC/SA-Zn^{2+}, and LE. (d) Graphic illustration, (e) cycling stability at 1 A/g, (f) CV curves at 0.1 mV s^{-1}, (g) GCD curves and (h) rate performance of the Zn-MnO$_2$ batteries with CMC/SA-Zn^{2+} hydrogel electrolyte at room temperature.

(FZMBs, Fig. 5d). The synthesis of α-MnO$_2$ nanorods with exceptional stability in cycling batteries has been achieved through a facile hydrothermal method as in previous studies. XRD pattern presented in Fig. S14 (Supporting Information) reveals the absence of impurity peaks, and all distinct peaks correspond well to the standard crystalline phase of α-MnO$_2$ (JCPDS: 01–072-1982). Furthermore, the SEM analysis indicated that the α-MnO$_2$ nanorods possess an average diameter of approximately 30–40 nm and exhibit a relatively uniform quasi-one-dimensional stick-like morphology (Fig. S15, Supporting Information). The unique shape of these nanorods may allow for efficient charge transfer and can directly utilize for fabrication of FZMBs to enhance the overall performance.

The electrochemical behavior of as-assembled Zn-MnO$_2$ batteries during their initial five cycles was investigated using cyclic voltammetry (CV), with a voltage range of 0.8–1.8 V examined (Fig. 5f). In the first cycle, a reduction peak at approximately 1.16 V and an oxidation peak at 1.61 V were observed, indicating a visible discharge/charge plateaus pair that suggests the process of Zn^{2+} insertion and extraction [38,73]. The subsequent cycle exhibits cathodic peaks at 1.27 V and 1.38 V, along with anodic peaks at 1.57 V and 1.65 V. This phenomenon presents compelling evidence supporting the co-insertion mechanism of H$^+$ and Zn^{2+} in the Zn-MnO$_2$ batteries that employed the CMC/SA-Zn^{2+} hydrogel electrolyte. According to previous studies, the observed pair of new redox peaks can be attributed to H$^+$ insertion-extraction [73,74]. Furthermore, the basically overlapping of the CV curves in subsequent cycles indicates that the battery exhibits a high level of stability during

discharge and charge process. The galvanostatic charge/discharge (GCD) curve at different current densities and the corresponding rate capabilities were given in Fig. 5g and Fig. 5h. The quasi-solid-state Zn-MnO$_2$ battery exhibits a specific discharge capacity of 218 mAh/g at a current density of 0.2 A/g (Fig. 5h). Even as the current density increases to 2 A/g, it maintains a capacity of 57.5 mAh/g. The highlighted rate performance of MnO$_2$/CMC/SA-Zn^{2+}/Zn batteries can be attributed to the aforementioned analytical factors: (1) The presence of charged groups within CMC/SA-Zn^{2+} can regulate the uniform distribution of Zn^{2+}, thereby effectively promoting the development of a more continuous and dendrite-free Zn anode during prolonged deposition/stripping process. (2) The 3D cross-linked network of CMC/SA-Zn^{2+} exhibits a highly porous architecture, which contributes to enhanced ionic conductivity. (3) The hydrophilic groups in the skeleton, combined with the strong complexation between Zn^{2+} and COO$^-$, enhance compatibility between the quasi-solid-state electrolyte and electrode. Consequently, efficient transport of zinc ions across the electrolyte interface is achieved, leading to outstanding rate capability for MnO$_2$/CMC/SA-Zn^{2+}/Zn batteries. Moreover, after undergoing 500 cycles at 1 A/g, the quasi-solid-state battery shows high coulombic efficiency close to 100 %, with its specific capacity eventually stabilizing at 77.2 mAh/g (Fig. 5e). The Jahn-teller effect of MnO$_2$ is noteworthy as it leads to the dissolution of Mn^{2+} in the electrolyte, resulting in a decline in capacity [75,76]. To enhance the cycle stability of MnO$_2$, current efforts primarily focus on mitigating Mn^{2+} dissolution through nano-engineering [77], doping modification [78], defect engineering [79], crystal

structure regulation of manganese oxide [80], and surface coating construction [76]. The aforementioned findings suggest potential avenues for enhancing the cycle stability of MnO_2 and optimizing the capacity of the full-cell. We anticipate that further modifications to MnO_2 in our future research endeavors will yield improvements in the electrochemical performance of flexible Zn-MnO_2 batteries.

3.5. Self-healing property and dynamic stability of the FZMB

The self-healing property effectively safeguards the flexible batteries against localized stress caused by various deformations during their daily usage, thereby significantly prolonging the lifespan and enhancing the reliability of the electronic system. Here, the FZMB was cut into two parts. It can be observed that the surface of the fracture area contains a majority of hydroxyl and carbonyl groups in the CMC/SA-Zn^{2+} hydrogel electrolyte (Fig. 6a). Upon reconnection of the broken FZMB, molecular interaction such as hydrogen bonds and coordination bonds are re-established along the fractured region (Fig. 6a), thereby restoring both mechanical properties and ion transmissions in the CMC/SA-Zn^{2+} hydrogel electrolyte (Fig. 2e–g, Fig. S6, Supporting Information). With the effective self-repairing of the CMC/SA-Zn^{2+} hydrogel electrolyte, the FZMB can be revitalized as both the α-MnO_2 cathode and Zn anode

regain their connection (Fig. 6b, c). Subsequently, a comparison of the CV curves before and after self-healing demonstrates almost no deviation from the origin state and near-complete restoration of device functionality (Fig. 6b). Moreover, we tested the self-healing ability by cutting the entire device and recontacting its segments (Fig. 6c). By connecting two devices in series, they are capable of powering an LED. If one segment of the device is disconnected, the LED will turn off; Once both segments are reconnected, it immediately resumes operation, showcasing the excellent self-healing properties of our battery. It also implies that the self-healed CMC/SA-Zn^{2+} hydrogel electrolyte induce electrode recontact and recover both electronic and ionic conduction.

Hence, it is unsurprising that the self-healed FZMB exhibits the ability to restore its electrochemical properties and power electronic devices even when subjected to significant physical harm such as cutting, bending, soaking, and washing. This stands in stark contrast to conventional coin, rectangular, or cylindrical batteries which are vulnerable to damage. To further assess the practical value of FZMBs, different bending angles were tested on the battery device as depicted in Fig. 6d. The FZMBs can withstand bending up to 180°, and the decrease in capacity is barely perceptible, thereby confirming the safety performance and good flexibility of the battery. Moreover, in the event of certain operational accidents, the FZMBs may encounter a significant
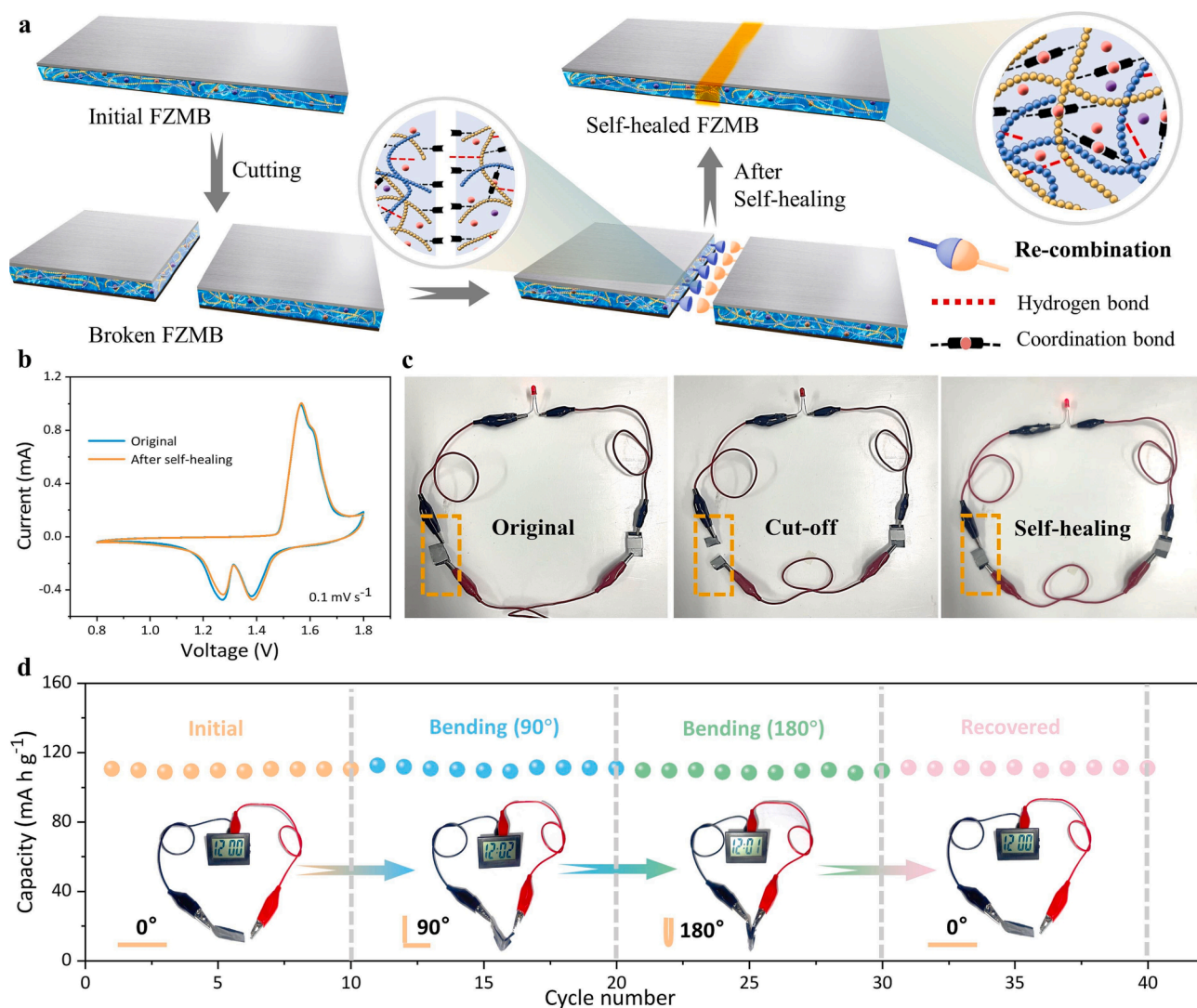
Fig. 6. (a) Illustration of the self-healing process of the FZMB. (b) CV curves of the FZMB before and after cutting/self-healing at 0.1 mV s^{-1}. (c) Photographs of the two self-healed FZMBs in series powering an LED. (d) Cycle performance of the FZMBs after bending to different angles. Inset: Corresponding optical photos of an electric clock powered by the FZMBs under various bending angles.

amount of water. To evaluate the waterproof and stability of the FZMB, we submerge and rinse the FZMBs in a plastic container for one hour (Fig. S16, Supporting Information). It can be seen that the electronic meter still functions normally when paired with the FZMBs. Furthermore, by cutting off two sections of FZMBs and then submerging them in deionized water (Fig. S17, Supporting Information), the FZMBs are still able to power device as usual, demonstrating a highlighted mechanical stability, waterproofing capabilities, and adhesion force of CMC/SA-Zn^{2+} hydrogel electrolyte.

4. Conclusion

In summary, we have developed a natural polymer-based hydrogel electrolyte named CMC/SA-Zn^{2+} with self-repairability for high-performance flexible Zn-MnO_2 batteries (FZMBs). In this functional electrolyte, Zn^{2+} can operate as both an ion-conducting agent and a cross-linking agent to facilitate the creation of the interpenetrated double cross-linked structure, which effectively improves the mechanical properties and prolongs the lifespan of Zn electrode by inhibiting Zn corrosion, HER and dendrite growth. As a result, the CMC/SA-Zn^{2+} shows a higher fracture stress up to 1.42 MPa with comparable stretchability, and the corresponding symmetrical cell exhibits an ultra-long cycle life of up to 2000 h. Impressively, the CMC/SA-Zn^{2+} hydrogel electrolyte has a high stable voltage of 2.4 V due to the abundance of hydrophilic and zincophilic charged groups. A quasi-solid full cell with CMC/SA-Zn^{2+} as the electrolyte and α-MnO_2 as the cathode shows excellent cycling stability of 500 cycles with high coulombic efficiency close to 100 %. Importantly, by leveraging the supramolecular interactions of Zn^{2+}–COO^- and internal hydrogen bonds, the self-healed CMC/SA-Zn^{2+} hydrogel electrolyte exhibits enhanced resilience against mechanical damage during idle periods and operation. Furthermore, the FZMBs with CMC/SA-Zn^{2+} enables the provision of unfluctuating or uninterrupted and stable power supply to electronic devices, even under severe conditions like tailoring, bending and washing. This suggests a promising potential for flexible energy storage applications in the future. Our work sheds new light on paving the way for designing the next generation of promising and environmentally friendly FZMBs and other wearable energy storage devices.

CRediT authorship contribution statement

Yanping Yang: Writing – review & editing, Writing – original draft, Visualization, Validation, Supervision, Software, Resources, Project administration, Methodology, Investigation, Formal analysis, Data curation, Conceptualization. **Luwei Shi:** Writing – original draft, Methodology, Investigation, Data curation. **Yaqi Wu:** Methodology, Data curation. **Zhehua Chen:** Funding acquisition, Visualization. **Xinyuan Zhu:** Supervision, Project administration, Funding acquisition. **Lijun Du:** Project administration, Funding acquisition. **Youfu Wang:** Writing – review & editing, Project administration, Funding acquisition, Conceptualization.

Declaration of competing interest

The authors declare that they have no known competing financial interests or personal relationships that could have appeared to influence the work reported in this paper.

Data availability

Data will be made available on request.

Acknowledgements

Appendix A. Supplementary data

Supplementary data to this article can be found online at https://doi.org/10.1016/j.cej.2024.149780.

References

[1] Y. Yang, W. Li, W. Su, M. Lang, H. Li, F. Zhang, Multiple healing flexible zinc-ion battery based on double cross-linked polyampholyte hydrogel electrolyte, J. Power Sources 579 (2023) 233274, https://doi.org/10.1016/j.jpowsour.2023.233313.

[2] H. Lu, J. Hu, J. Wei, K. Zhang, X. Xiao, J. Zhao, Q. Hu, J. Yu, G. Zhou, B. Xu, A recyclable biomass electrolyte towards green zinc-ion batteries, Nat. Commun. 14 (1) (2023) 4435, https://doi.org/10.1038/s41467-023-40178-0.

[3] L. Hong, X.M. Wu, Y.S. Liu, C.Y. Yu, Y.C. Liu, K.X. Sun, C.Y. Shen, W. Huang, Y. F. Zhou, J.S. Chen, K.X. Wang, Self-adapting and self-healing hydrogel interface with fast Zn^{2+} transport kinetics for highly reversible zn anodes, Adv. Funct. Mater. 33 (2023) 2300952, https://doi.org/10.1002/adfm.202300952.

[4] H. Xu, Q. Zhu, Y. Zhao, Z. Du, B. Li, S. Yang, Phase-changeable dynamic conformal electrode/electrolyte interlayer enabling pressure-independent solid-state lithium metal batteries, Adv. Mater. 35 (18) (2023) e2212111, https://doi.org/10.1002/adma.202212111.

[5] J. Chen, G. Adit, L. Li, Y. Zhang, D.H.C. Chua, P.S. Lee, Optimization strategies toward functional sodium-ion batteries, Energy Environ. Mater. 6 (4) (2023) e12633, https://doi.org/10.1002/eem2.12633.

[6] N.M. Badawi, K.M. Batoo, R. Subramaniam, R. Kasi, S. Hussain, A. Imran, M. Muthuramamoorthy, Highly conductive and reusable cellulose hydrogels for supercapacitor applications, Micromachines 14 (7) (2023) 1461, https://doi.org/10.3390/mi14071461.

[7] C. Gu, M. Wang, K. Zhang, J. Li, Y.L. Lu, Y. Cui, Y. Zhang, C.S. Liu, A full-device autonomous self-healing stretchable soft battery from self-bonded eutectogels, Adv. Mater. 35 (6) (2022) e2208392, https://doi.org/10.1002/adma.202208392.

[8] L. Ma, Q. Li, Y. Ying, F. Ma, S. Chen, Y. Li, H. Huang, C. Zhi, Toward practical high-areal-capacity aqueous zinc-metal batteries: quantifying hydrogen evolution and a solid-ion conductor for stable zinc anodes, Adv. Mater. 33 (12) (2021) e2007406, https://doi.org/10.1002/adma.202007406.

[9] C. Dai, X. Jin, H. Ma, L. Hu, G. Sun, H. Chen, Q. Yang, M. Xu, Q. Liu, Y. Xiao, X. Zhang, H. Yang, Q. Guo, Z. Zhang, L. Qu, Maximizing energy storage of flexible aqueous batteries through decoupling charge carriers, Adv. Energy Mater. 11 (14) (2021) 2003982, https://doi.org/10.1002/aenm.202003982.

[10] C. Dai, L. Hu, X. Jin, H. Chen, X. Zhang, S. Zhang, L. Song, H. Ma, M. Xu, Y. Zhao, Z. Zhang, H. Cheng, L. Qu, A cascade battery: coupling two sequential electrochemical reactions in a single battery, Adv. Mater. 33 (44) (2021) e2105480, https://doi.org/10.1002/adma.202105480.

[11] H. Pan, Y. Shao, P. Yan, Y. Cheng, K.S. Han, Z. Nie, C. Wang, J. Yang, X. Li, P. Bhattacharya, K.T. Mueller, J. Liu, Reversible aqueous zinc/manganese oxide energy storage from conversion reactions, Nat. Energy 1 (5) (2016) 16039, https://doi.org/10.1038/nenergy.2016.39.

[12] D. Kundu, B.D. Adams, V. Duffort, S.H. Vajargah, L.F. Nazar, A high-capacity and long-life aqueous rechargeable zinc battery using a metal oxide intercalation cathode, Nat. Energy 1 (10) (2016) 1, https://doi.org/10.1038/nenergy.2016.119.

[13] F. Hu, M. Li, G. Gao, H. Fan, L. Ma, The gel-state electrolytes in zinc-ion batteries, Batteriesl 8 (11) (2022) 214, https://doi.org/10.3390/batteries8110214.

[14] H. Li, Y. Liu, Z. Chen, Y. Yang, T. Lv, T. Chen, High voltage and healing flexible zinc ion battery based on ionogel electrolyte, J. Colloid Interface Sci. 639 (2023) 408–415, https://doi.org/10.1016/j.jcis.2023.01.088.

[15] H. Wang, W. Wei, X. Liu, S. Xu, Y. Dong, R. He, Ultrahigh-capacity epitaxial deposition of planar zn flakes enabled by amino-rich adhesive hydrogel electrolytes for durable low-temperature zinc batteries, Energy Storage Mater. 55 (2023) 597–605, https://doi.org/10.1016/j.ensm.2022.12.023.

[16] Z. Gong, Z. Li, P. Wang, K. Jiang, Z. Bai, K. Zhu, J. Yan, K. Ye, G. Wang, D. Cao, G. Chen, Conductive framework-stabilized zn-metal anodes for high-performance zn-ion batteries and capacitors, Energy Mater. Adv. 4 (2023) 0035, https://doi.org/10.34133/energymatadv.0035.

[17] Y. Mao, Z. Li, Y. Li, D. Cao, G. Wang, K. Zhu, G. Chen, Breaking intramolecular hydrogen bonds of polymer films to enable dendrite-free and hydrogen-suppressed zinc metal anode, Chem. Eng. J. 461 (2023) 141707, https://doi.org/10.1016/j.cej.2023.141707.

[18] D. Liu, Z. Tang, L. Luo, W. Yang, Y. Liu, Z. Shen, X.-H. Fan, Self-healing solid polymer electrolyte with high ion conductivity and super stretchability for all-solid zinc-ion batteries, ACS Appl. Mater. Interfaces 13 (30) (2021) 36320–36329, https://doi.org/10.1021/acsami.1c09200.

[19] J. Liu, J. Long, Z. Shen, X. Jin, T. Han, T. Si, H. Zhang, A self-healing flexible quasi-solid zinc-ion battery using all-in-one electrodes, Adv. Sci. 8 (8) (2021) 2004689, https://doi.org/10.1002/advs.202004689.

[20] S. Huang, F. Wan, S. Bi, J. Zhu, Z. Niu, J. Chen, A self-healing integrated all-in-one zinc-ion battery, Angew. Chem. Int. Ed. 58 (13) (2019) 4313–4317, https://doi.org/10.1002/anie.201814653.

[21] X. Du, J. Shi, Z. Chen, T. Ni, J. Li, L. Ruan, W. Zeng, F. Cheng, Y. Yue, S. Wang, [8] A laser etched zinc ion microbattery with excellent flexibility and self-healability,

Sustainable Energy Fuels 4 (9) (2020) 4713–4721, https://doi.org/10.1039/d0se00843e.

[22] G. Li, Z. Zhao, S. Zhang, L. Sun, M. Li, J.A. Yuwono, J. Mao, J. Hao, J. Vongsvivut, L. Xing, C.-X. Zhao, Z. Guo, A biocompatible electrolyte enables highly reversible zn anode for zinc ion battery, Nat. Commun. 14 (1) (2023), https://doi.org/10.1038/s41467-023-42333-z.

[23] R. Zhang, Y. Tao, Q. Xu, N. Liu, P. Chen, Y. Zhou, Z. Bai, Rheological and ion-conductive properties of injectable and self-healing hydrogels based on xanthan gum and silk fibroin, Int. J. Biol. Macromol. 144 (2020) 473–482, https://doi.org/10.1016/j.ijbiomac.2019.12.132.

[24] T. Xu, K. Liu, N. Sheng, M. Zhang, W. Liu, H. Liu, L. Dai, X. Zhang, C. Si, H. Du, K. Zhang, Biopolymer-based hydrogel electrolytes for advanced energy storage/conversion devices: properties, applications, and perspectives, Energy Storage Mater. 48 (2022) 244–262, https://doi.org/10.1016/j.ensm.2022.03.013.

[25] M. Chen, J. Chen, W. Zhou, J. Xu, C.-P. Wong, High-performance flexible and self-healable quasi-solid-state zinc-ion hybrid supercapacitor based on borax-crosslinked polyvinyl alcohol/nanocellulose hydrogel electrolyte, J. Mater. Chem. A 7 (46) (2019) 26524–26532, https://doi.org/10.1039/c9ta10944g.

[26] J. Zhao, K.K. Sonigara, J. Li, J. Zhang, B. Chen, J. Zhang, S.S. Soni, X. Zhou, G. Cui, L. Chen, A Smart Flexible Zinc Battery with Cooling Recovery Ability, Angew. Chem., Int. Ed. 56(27) (2017) 7871-7875. https://doi.org/https://doi.org/10.1002/anie.201704373.

[27] Y. Li, Y. Yang, X. Liu, C. Chen, C. Qian, L. Han, Q. Han, Highly sensitive and wearable self-powered sensors based on a stretchable hydrogel comprising dynamic hydrogen bond and dual coordination bonds, Colloids Surf., A 628 (2021) 127336, https://doi.org/10.1016/j.colsurfa.2021.127336.

[28] Q. Chen, J. Zhao, Z. Chen, Y. Jin, J. Peng, Y. Chen, Y. Qiu, Y. Huang, Self-healable zwitterionic double-network hydrogels as electrolyte for zinc-ion hybrid supercapacitor/battery, Int. J. Hydrogen Energy 47 (57) (2022) 23909–23918, https://doi.org/10.1016/j.ijhydene.2022.05.195.

[29] W. Ling, F. Mo, J. Wang, Q. Liu, Y. Liu, Q. Yang, Y. Qiu, Y. Huang, Self-healable hydrogel electrolyte for dendrite-free and self-healable zinc-based aqueous batteries, Today Phys. 20 (2021) 100458, https://doi.org/10.1016/j.mtphys.2021.100458.

[30] Y. Shao, J. Zhao, W. Hu, Z. Xia, J. Luo, Y. Zhou, L. Zhang, X. Yang, N. Ma, D. Yang, Q. Shi, J. Sun, L. Zhang, J. Hui, Y. Shao, Regulating interfacial ion migration via wool keratin mediated biogel electrolyte toward robust flexible zn-ion batteries, Small 18 (10) (2022) e2107163, https://doi.org/10.1002/smll.202107163.

[31] L. Zhao, J. Fu, Z. Du, X. Jia, Y. Qu, F. Yu, J. Du, Y. Chen, High-strength and flexible CELLULOSE/PEG based gel polymer electrolyte with high performance for lithium ion battery, J. Membr. Sci. 593 (2020), https://doi.org/10.1016/j.memsci.2019.117428.

[32] F. Yu, H. Zhang, L. Zhao, Z. Sun, Y. Li, Y. Mo, Y. Chen, A flexible cellulose/methylcellulose gel polymer electrolyte endowing superior Li(+) conducting property for lithium ion battery, Carbohydr Polym 246 (2020) 116622, https://doi.org/10.1016/j.carbpol.2020.116622.

[33] W. Xie, Y. Dang, L. Wu, W. Liu, A. Tang, Y. Luo, Experimental and molecular simulating study on promoting electrolyte-immersed mechanical properties of cellulose/lignin separator for lithium-ion battery, Polym. Test 90 (2020) 106773, https://doi.org/10.1016/j.polymertesting.2020.106773.

[34] M. Chen, J. Chen, W. Zhou, X. Han, Y. Yao, C.-P. Wong, Realizing an all-round hydrogel electrolyte toward environmentally adaptive dendrite-free aqueous zn-MnO2 batteries, Adv. Mater. 33 (9) (2021) 2007559, https://doi.org/10.1002/adma.202007559.

[35] Y.S. Zhu, S.Y. Xiao, M.X. Li, Z. Chang, F.X. Wang, J. Gao, Y.P. Wu, Natural macromolecule based carboxymethyl cellulose as a gel polymer electrolyte with adjustable porosity for lithium ion batteries, J. Power Sources 288 (2015) 368–375, https://doi.org/10.1016/j.jpowsour.2015.04.117.

[36] Y. Huang, J. Liu, J. Wang, M. Hu, F. Mo, G. Liang, C. Zhi, An intrinsically self-healing NiCo, zn rechargeable battery with a self-healable ferric-ion-crosslinking sodium polyacrylate hydrogel electrolyte, Angew. Chem. Int. Ed. 57 (31) (2018) 9810–9813, https://doi.org/10.1002/anie.201805618.

[37] Q. Li, X. Cui, Q. Pan, Self-healable hydrogel electrolyte toward high-performance and reliable quasi-solid-state zn-MnO2 batteries, ACS Appl. Interfaces 11 (42) (2019) 38762–38770, https://doi.org/10.1021/acsami.9b13553.

[38] Y. Hu, P. Shen, N. Zeng, L. Wang, D. Yan, L. Cui, K. Yang, C. Zhai, Hybrid hydrogel electrolyte based on metal-organic supermolecular self-assembly and polymer chemical cross-linking for rechargeable aqueous zn-MnO2 batteries, ACS Appl. Mater. Interfaces 12 (37) (2020) 42285–42293, https://doi.org/10.1021/acsami.0c10321.

[39] X. Lin, X. Jin, X. Guo, X. Jia, All-carboxymethyl cellulose sponges for removal of heavy metal ions, Cellulose 28 (5) (2021) 3113–3122, https://doi.org/10.1007/s10570-021-03685-1.

[40] X. Lin, M. Wang, J. Zhao, X. Wu, J. Xie, J. Yang, Super-tough and self-healable all-cellulose-based electrolyte for fast degradable quasi-solid-state supercapacitor, Carbohydr. Polym. 304 (2023) 120502, https://doi.org/10.1016/j.carbpol.2022.120502.

[41] H. Huang, L. Han, X. Fu, Y. Wang, Z. Yang, L. Pan, M. Xu, A powder self-healable hydrogel electrolyte for flexible hybrid supercapacitors with high energy density and sustainability, Small 17 (10) (2021) 2006807, https://doi.org/10.1002/smll.202006807.

[42] Y. Liu, A. Gao, J. Hao, X. Li, J. Ling, F. Yi, Q. Li, D. Shu, Soaking-free and self-healing hydrogel for wearable zinc-ion batteries, Chem. Eng. J. 452 (2023) 139605, https://doi.org/10.1016/j.cej.2022.139605.

[43] G. Kresse, J. Furthmüller, Efficiency of ab-initio total energy calculations for metals and semiconductors using a plane-wave basis set, Comp. Mater. Sci. 6 (1) (1996) 15–50.

[44] J.P. Perdew, K. Burke, M. Ernzerhof, Ernzerhof, generalized gradient approximation made simple, Phys. Rev. Lett. 77 (18) (1996) 3865, https://doi.org/10.1103/PhysRevLett.77.3865.

[45] P.E. Blochl, Projector augmented-wave method, Phys. Rev. B 50 (24) (1994) 17953–17979, https://doi.org/10.1103/physrevb.50.17953.

[46] S. Grimme, Semiempirical GGA-type density functional constructed with a long-range dispersion correction, J. Comput. Chem. 27 (15) (2006) 1787–1799, https://doi.org/10.1002/jcc.20495.

[47] G. Ji, R. Hu, Y. Wang, J. Zheng, High energy density, flexible, low temperature resistant and self-healing zn-ion hybrid capacitors based on hydrogel electrolyte, J. Energy Storage 46 (2022) 103858, https://doi.org/10.1016/j.est.2021.103858.

[48] M.S. Kim, J.W. Kim, J. Yun, Y.R. Jeong, S.W. Jin, G. Lee, H. Lee, D.S. Kim, K. Keum, J.S. Ha, A rationally designed flexible self-healing system with a high performance supercapacitor for powering an integrated multifunctional sensor, Appl. Surf. Sci. 515 (2020) 146018, https://doi.org/10.1016/j.apsusc.2020.146018.

[49] K. Leng, G. Li, J. Guo, X. Zhang, A. Wang, X. Liu, J. Luo, A safe polyzwitterionic hydrogel electrolyte for long-life quasi-solid state zinc metal batteries, Adv. Funct. Mater. 30 (23) (2020) 2001317, https://doi.org/10.1002/adfm.202001317.

[50] E. Garcia-Gaitan, D. Frattini, I.R. de Larramendi, M. Martinez-Ibanez, D. Gonzalez, M. Armand, N. Ortiz-Vitoriano, Flexible gel polymer electrolytes based on carboxymethyl cellulose blended with polyvinyl alcohol or polyacrylic acid for zinc-air batteries, Batteries Supercaps 6 (2023) e202200570, https://doi.org/10.1002/batt.202200570.

[51] X. He, L. Zeng, X. Cheng, C. Yang, J. Chen, H. Chen, H. Ni, Y. Bai, W. Yu, K. Zhao, P. Hu, Shape memory composite hydrogel based on sodium alginate dual crosslinked network with carboxymethyl cellulose, Eur. Polym. J. 156 (2021) 110592, https://doi.org/10.1016/j.eurpolymj.2021.110592.

[52] Y. Li, Y. Yang, X. Liu, Y. Wu, L. Han, Q. Han, Flexible self-powered integrated sensing system based on a rechargeable zinc-ion battery by using a multifunctional polyacrylamide/carboxymethyl chitosan/LiCl ionic hydrogel, Colloids Surf., A 648 (2022). https://doi.org/10.1016/j.colsurfa.2022.129254.

[53] C.K. Karan, S. Mallick, C.R. Raj, M. Bhattacharjee, A self-healing metal-organic hydrogel for an all-solid flexible supercapacitor, Chem. Eur. J. 25 (65) (2019) 14775–14779, https://doi.org/10.1002/chem.201903561.

[54] J.C. Lai, X.Y. Jia, D.P. Wang, Y.B. Deng, P. Zheng, C.H. Li, J.L. Zuo, Z. Bao, Thermodynamically stable whilst kinetically labile coordination bonds lead to strong and tough self-healing polymers, Nat. Commun. 10 (1) (2019) 1164, https://doi.org/10.1038/s41467-019-09130-z.

[55] Q. Liu, R. Chen, L. Xu, Y. Liu, Y. Dai, M. Huang, L. Mai, Steric molecular combing effect enables ultrafast self-healing electrolyte in quasi-solid-state zinc-ion batteries, ACS Energy Lett. 7 (8) (2022) 2825–2832, https://doi.org/10.1021/acsenergylett.2c01459.

[56] Q. Fu, S. Hao, X. Zhang, H. Zhao, F. Xu, J. Yang, All-round supramolecular zwitterionic hydrogel electrolytes enabling environmentally adaptive dendrite-free aqueous zinc ion capacitors, Energy Environ. Sci 16 (2023) 1291, https://doi.org/10.1039/d2ee03793a.

[57] X. Zhang, T. Liao, T. Long, Y.-K. Cao, X.-X. Zeng, Q. Deng, B. Liu, X.-W. Wu, Y.-P. Wu, In situ buildup of zinc anode protection films with natural protein additives for high-performance zinc battery cycling, ACS Appl. Mater. Interfaces 15 (2023) 32496, https://doi.org/10.1021/acsami.3c06907.

[58] X. Zhang, C. Jia, J. Zhang, L. Zhang, X. Liu, Smart aqueous zinc ion battery: operation principles and design strategy, Adv. Sci. 11 (2023) 2305201, https://doi.org/10.1002/advs.202305201.

[59] G. Li, L. Sun, S. Zhang, C. Zhang, H. Jin, K. Davey, G. Liang, S. Liu, J. Mao, Z. Guo, Developing cathode materials for aqueous zinc ion batteries: challenges and practical prospects, Adv. Funct. Mater. (2023) 2301291, https://doi.org/10.1002/adfm.202301291.

[60] Y.X. Li, J.X. Zhao, Q. Hu, T.W. Hao, H. Cao, X.M. Huang, Y. Liu, Y.Y. Zhang, D. M. Lin, Y.X. Tang, Y.Q. Cai, Prussian blue analogs cathodes for aqueous zinc ion batteries, Mater. Today Energy 29 (2022) 101095, https://doi.org/10.1016/j.mtener.2022.101095.

[61] L.T. Ma, S.M. Chen, C.B. Long, X.L. Li, Y.W. Zhao, Z.X. Liu, Z.D. Huang, B.B. Dong, J.A. Zapien, C.Y. Zhi, Achieving high-voltage and high-capacity aqueous rechargeable zinc ion battery by incorporating two-species redox reaction, Adv. Energy Mater. 9 (45) (2019) 1902446, https://doi.org/10.1002/aenm.201902446.

[62] N. Wang, R. Zhou, Z. Zheng, T. Xin, M. Hu, B. Wang, J. Liu, Flexible solid-state zn-polymer batteries with practical functions, Chem. Eng. J. 425 (2021) 131454, https://doi.org/10.1016/j.cej.2021.131454.

[63] L.J. Kong, M. Liu, H. Huang, Y.H. Xu, X.H. Bu, Metal/covalent-organic framework based cathodes for metal-ion batteries, Adv. Energy Mater. 12 (4) (2022) 00172, https://doi.org/10.1002/aenm.202100172.

[64] W.B. Liu, J.W. Hao, C.J. Xu, J. Mou, L.B. Dong, F.Y. Jiang, Z. Kang, J.L. Wu, B. Z. Jiang, F.Y. Kang, Investigation of zinc ion storage of transition metal oxides, sulfides, and borides in zinc ion battery systems, Chem. Commun. (cambridge, u. k.) 53 (51) (2017) 6872–6874, https://doi.org/10.1039/c7cc01064h.

[65] L. Wang, S. Yan, C.D. Quilty, J. Kuang, M.R. Dunkin, S.N. Ehrlich, L. Ma, K. J. Takeuchi, E.S. Takeuchi, A.C. Marschilok, Achieving stable molybdenum oxide cathodes for aqueous zinc-ion batteries in water-in-salt electrolyte, Adv. Mater. Interfaces 8 (9) (2021) 2002080, https://doi.org/10.1002/admi.202002080.

[66] J. Wu, J.L. Meng, Z.H. Yang, H.Z. Chen, Y. Rong, L. Deng, Z.M. Fu, Energy storage mechanism and electrochemical performance of Cu2O/rGO as advanced cathode for aqueous zinc ion batteries, J. Alloys Compd. 895 (2022) 162653, https://doi.org/10.1016/j.jallcom.2021.162653.

[67] J.P. Yan, E.H. Ang, Y. Yang, Y.F. Zhang, M.H. Ye, W.C. Du, C.C. Li, High-voltage zinc-ion batteries: design strategies and challenges, Adv. Funct. Mater. 31 (22) (2021) 2010213, https://doi.org/10.1002/adfm.202010213.

[68] F. Wan, Y. Zhang, L.L. Zhang, D.B. Liu, C.D. Wang, L. Song, Z.Q. Niu, J. Chen, Reversible oxygen redox chemistry in aqueous zinc-ion batteries, Angew. Chem., Int. Ed. 58 (21) (2019) 7062–7067, https://doi.org/10.1002/anie.201902679.

[69] Y. Lyu, J.A. Yuwono, P. Wang, Y. Wang, F. Yang, S. Liu, S. Zhang, B. Wang, K. Davey, J. Mao, Z. Guo, Organic pH buffer for dendrite-free and shuttle-free zn-I₂ batteries, Angew. Chem., Int. Ed. 62 (21) (2023) e202303011, https://doi.org/10.1002/anie.202303011.

[70] L.J. Yan, S.J. Zhang, Q.L. Kang, X.H. Meng, Z.H. Li, T.F. Liu, T.L. Ma, Z. Lin, Iodine conversion chemistry in aqueous batteries: challenges, strategies, and perspectives, Energy Storage Mater. 54 (2023) 339–365, https://doi.org/10.1016/j.ensm.2022.10.027.

[71] P. Shen, Y. Hu, S. Ji, H. Luo, C. Zhai, K. Yang, A self-healing nanocomposite hydrogel electrolyte for rechargeable aqueous zn-MnO2 battery, Colloids Surf., A 647 (2022) 129195, https://doi.org/10.1016/j.colsurfa.2022.129195.

[72] W. Xu, K. Zhao, W. Huo, Y. Wang, G. Yao, X. Gu, H. Cheng, L. Mai, C. Hu, X. Wang, Diethyl ether as self-healing electrolyte additive enabled long-life rechargeable aqueous zinc ion batteries, Nano Energy 62 (2019) 275–281, https://doi.org/10.1016/j.nanoen.2019.05.042.

[73] H. Ren, J. Zhao, L. Yang, Q. Liang, S. Madhavi, Q. Yan, Inverse opal manganese dioxide constructed by few-layered ultrathin nanosheets as high-performance cathodes for aqueous zinc-ion batteries, Nano Research 12 (6) (2019) 1347–1353, https://doi.org/10.1007/s12274-019-2303-1.

[74] W. Sun, F. Wang, S. Hou, C. Yang, X. Fan, Z. Ma, T. Gao, F. Han, R. Hu, M. Zhu, C. Wang, Zn/MnO2 battery chemistry with H+ and Zn2+ coinsertion, J. Am. Chem. Soc. 139 (29) (2017) 9775–9778, https://doi.org/10.1021/jacs.7b04471.

[75] X. Xu, X. Feng, M. Li, J. Yin, J. Chen, F. Li, W. Shi, Y. Cheng, J. Wang, Overcoming challenges: extending cycle life of aqueous zinc-ion batteries at high zinc utilization through a synergistic strategy, Small (2023) 2308273, https://doi.org/10.1002/smll.202308273.

[76] X. Xiao, L. Zhang, W. Xin, M. Yang, Y. Geng, M. Niu, H. Zhang, Z. Zhu, Self-assembled layer of organic phosphonic acid enables highly stable MnO2 cathode for aqueous znic batteries, Small (2024) 2309271, https://doi.org/10.1002/smll.202309271.

[77] R. Liu, S.B. Lee, MnO2/Poly(3,4-ethylenedioxythiophene) coaxial nanowires by one-step coelectrodeposition for electrochemical energy storage, J. Am. Chem. Soc. 130 (10) (2008) 2942–2943, https://doi.org/10.1021/ja7112382.

[78] G.G. Yadav, J.W. Gallaway, D.E. Turney, M. Nyce, J. Huang, X. Wei, S. Banerjee, Regenerable cu-intercalated MnO2 layered cathode for highly cyclable energy dense batteries, Nat. Commun. 8 (2017) 14424, https://doi.org/10.1038/ncomms14424.

[79] W. Qu, Y. Cai, B. Chen, M. Zhang, Heterointerface engineering-induced oxygen defects for the manganese dissolution inhibition in aqueous zinc ion batteries, Energy Environ. Mater. (2023) e12645, https://doi.org/10.1002/eem2.12645.

[80] C. Zhu, G. Fang, S. Liang, Z. Chen, Z. Wang, J. Ma, H. Wang, B. Tang, X. Zheng, J. Zhou, Electrochemically induced cationic defect in MnO intercalation cathode for aqueous zinc-ion battery, Energy Storage Mater. 24 (2020) 394–401, https://doi.org/10.1016/j.ensm.2019.07.030.